Neuron

Article

Genome-wide study reveals novel roles for formin-2 in axon regeneration as a microtubule dynamics regulator and therapeutic target for nerve repair

Graphical abstract

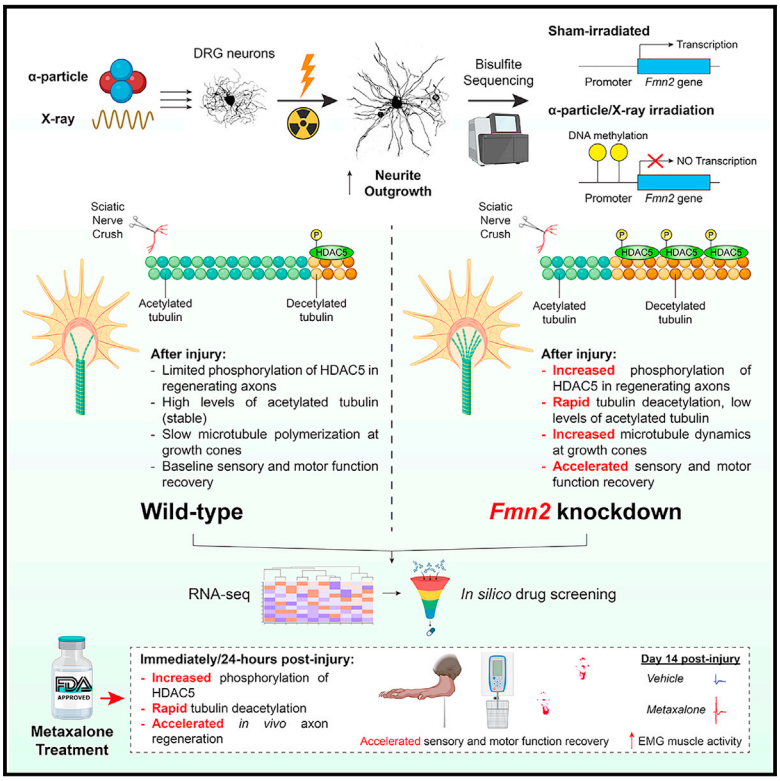

Highlights

- LDIR promotes intrinsic axonal growth, function recovery, and Fmn2 hypermethylation
- Fmn2 as a regulator of injury response, axon regeneration, and microtubule dynamics
- *Fmn2* deletion promotes axon regeneration via HDAC5-mediated tubulin deacetylation
- FDA drug metaxalone recapitulates growth-promoting effects of *Fmn2* deletion for PNI

Authors

Ngan Pan Bennett Au, Tan Wu, Xinyu Chen, ..., Giovanni Coppola, Xin Wang, Chi Him Eddie Ma

Correspondence

eddiema@cityu.edu.hk

In brief

Proximal peripheral nerve injury (PNI) results in poor clinical outcomes. Au et al. reveal that ionizing radiation induces intrinsic growth of injured neurons and *Fmn2* downregulation. *Fmn2* deletion enhances microtubule dynamics, axon regeneration, and function recovery. Using gene signature of *Fmn2* deletion identifies FDA-approved metaxalone recapitulating growth-promoting effects of *Fmn2* deletion for PNI.

Au et al., 2023, Neuron *111*, 3970–3987
December 20, 2023
https://doi.org/10.1016/j.neuron.2023.11.011

CellPress

CellPress

Neuron

Article

Genome-wide study reveals novel roles for formin-2 in axon regeneration as a microtubule dynamics regulator and therapeutic target for nerve repair

Ngan Pan Bennett Au,[1] Tan Wu,[2,3] Xinyu Chen,[1] Feng Gao,[2,3] Yuen Tung Yolanda Li,[1] Wing Yip Tam,[1] Kwan Ngok Yu,[4] Daniel H. Geschwind,[5,6] Giovanni Coppola,[5,6] Xin Wang,[2,3] and Chi Him Eddie Ma[1,7,*]

[1]Department of Neuroscience, City University of Hong Kong, Hong Kong, China
[2]Department of Surgery, The Chinese University of Hong Kong, Hong Kong, China
[3]Department of Biomedical Sciences, City University of Hong Kong, Hong Kong, China
[4]Department of Physics, City University of Hong Kong, Hong Kong, China
[5]Program in Neurogenetics, Department of Neurology, David Geffen School of Medicine, University of California, Los Angeles, Los Angeles, CA 90095, USA
[6]Department of Human Genetics, University of California, Los Angeles, Los Angeles, CA 90095, USA
[7]Lead contact
*Correspondence: eddiema@cityu.edu.hk
https://doi.org/10.1016/j.neuron.2023.11.011

SUMMARY

Peripheral nerves regenerate successfully; however, clinical outcome after injury is poor. We demonstrated that low-dose ionizing radiation (LDIR) promoted axon regeneration and function recovery after peripheral nerve injury (PNI). Genome-wide CpG methylation profiling identified LDIR-induced hypermethylation of the *Fmn2* promoter, exhibiting injury-induced Fmn2 downregulation in dorsal root ganglia (DRGs). Constitutive knockout or neuronal *Fmn2* knockdown accelerated nerve repair and function recovery. Mechanistically, increased microtubule dynamics at growth cones was observed in time-lapse imaging of *Fmn2*-deficient DRG neurons. Increased HDAC5 phosphorylation and rapid tubulin deacetylation were found in regenerating axons of neuronal *Fmn2*-knockdown mice after injury. Growth-promoting effect of neuronal *Fmn2* knockdown was eliminated by pharmaceutical blockade of HDAC5 or neuronal *Hdac5* knockdown, suggesting that *Fmn2*deletion promotes axon regeneration via microtubule post-translational modification. *In silico* screening of FDA-approved drugs identified metaxalone, administered either immediately or 24-h post-injury, accelerating function recovery. This work uncovers a novel axon regeneration function of Fmn2 and a small-molecule strategy for PNI.

INTRODUCTION

Injury to the peripheral nervous system (PNS) induces either adaptive (growth and survival) or maladaptive (cell death, neuropathic pain, and failure of regeneration) responses determined precisely by expression levels of a subset of genes (intrinsic growth program).[1–8] The first step for successful peripheral nerve regeneration is to induce axon regeneration from injured neurons. On the level of the cytoskeleton, this requires a precise balance between stable and dynamic microtubules, as is observed during neuronal development. Damage to the peripheral nerve is followed by a slow rate of axonal regrowth and associated with sub-optimal function recovery.[1,3,4,9,10] For instance, the most common type of proximal nerve injury in humans such as brachial plexus injury and those that involve complete transection of peripheral nerve require long-distance axon regeneration to reinnervate their target muscles. Function recovery is virtually non-existent even after surgical repair due largely to the slow rate of axonal regrowth and limited target muscle reinnervation.[3–5] One of the major challenges is, therefore, to identify gene(s) that are involved in this adaptive response.

DNA methylation is the most studied and common epigenetic modification in gene expression.[11,12] Recent reports have demonstrated that the orchestration of global DNA methylation and demethylation serve as fundamental mechanisms to promote axon regeneration.[13–17] Epigenetic regulators such as ten-eleven translocation methylcytosine dioxygenases (Tets) and ubiquitin-like containing PHD ring finger 1 (UHRF1) have been shown to be important for peripheral nerve regeneration. Tets are enzymes that regulate DNA demethylation, and their expression is increased in dorsal root ganglia (DRGs) after sciatic nerve injury. TET3 was highly upregulated in DRG neurons 1–3 days after sciatic nerve injury and promoted expression of multiple regeneration-associated genes (RAGs).[16,18] UHRF1 enhanced regenerative capacity

of DRG neurons through promoter methylation (gene silencing) of phosphatase and tensin homolog (PTEN) and RE1-silencing transcription factor (REST).[15] Nevertheless, the correlation between global DNA methylation and RAG expression after peripheral nerve injury (PNI) is weak and rather descriptive.[17–20] Inconclusive results are reported regarding the importance of DNA methylation after peripheral axonal injury. Pharmacological perturbation of the PNI-induced change in DNA methylation status (either activation or inhibition of DNA methylation) resulted in a marked attenuation of axonal regrowth in DRG neurons.[19] The administration of folate, which increased global DNA methylation in the spinal cord, enhanced axon regeneration of spinal neurons after spinal cord injury.[21] However, how the alternation of DNA methylation might functionally impact individual gene expression and orchestrate downstream effectors contributing to successful axon regeneration remains elusive.

Together with DNA methylation, histone modifications represent the classic and essential epigenetic mechanisms. Histone deacetylases (HDACs) are not only enzymes that catalyze deacetylation from histone in the nuclei but also from many cytoplasmic proteins such as α-tubulin. Post-translational modification of tubulin on microtubule dynamics, such as acetylation, is one of the key events in regulating axon regeneration.[22–28] A previous study reported that inhibition of microtubule dynamics without disrupting the integrity of axonal microtubules results in a reduction of axonal growth.[29] Tubulin is the major building block of microtubules. Stable and dynamic microtubules can be distinguished by the extent of tubulin acetylation along the axon shaft.[30] For instance, acetylated tubulins (stable) are mainly found in stable microtubules in the proximal segments of axons where active growth is limited. Highly deacetylated tubulins (dynamic) are located in the distal end of axons where active tubulin polymerization occurs at the growth cones.[30,31] PNI induces microtubule remodeling to facilitate the formation of growth cones and promote axon regeneration.[32] PNI induces tubulin deacetylation at the distal end of injured peripheral nerve where active axonal regrowth is taking place. The administration of scriptaid, a pan-HDAC inhibitor that blocks tubulin deacetylation in damaged axons, markedly stalled axonal regrowth after PNI.[23]

The beneficial effects of low-dose ionizing radiation (LDIR) have been documented for decades.[33–37] LDIR induces adaptive responses to enhance the overall functional ability of organisms and their intrinsic growth capacity.[37] The beneficial effects of LDIR such as X-ray on cell growth stimulation,[34] average life span extension in rodent,[38–40] neuroprotection in animal disease models, as well as in human leukemia disease[41,42] and Alzheimer's disease,[43,44] have been reported. Local low-dose X-ray irradiation of sciatic nerve improves nerve repair and function recovery in rats, although the mechanism remains unclear.[45] LDIR has been known to induce DNA methylation and transcriptional changes in different *in vitro* and *in vivo* models.[46–50] These studies suggest that alternation in gene expression profiling following LDIR contributes to the beneficial adaptive response in living organisms. Given that there is still much to learn before LDIR becomes a routine, effective, and safe medical treatment. Identifying key genes and small molecules that are associated with LDIR-induced protective effects could become an attractive and safe pharmacological treatment for PNIs.

To achieve this, we first showed that the two commonly used ionizing radiation sources, alpha-particle (α-particle) and X-ray, promoted neurite outgrowth in purified DRG neurons in cultures. Low-dose (LD) whole-body X-ray irradiation enhanced the intrinsic growth capacity of injured neurons and induced robust axon regeneration in axotomized DRG neurons in *ex vivo* explant cultures, as well as accelerated *in vivo* axon regeneration and function recovery after sciatic nerve crush injury. In-depth genome-wide CpG methylation profiling and bioinformatic analysis were performed to identify hypermethylation of *Formin-2* (*Fmn2*) promoter as the major contributor associated with the promoting effects of LDIR. To establish the role of Fmn2 in peripheral nerve regeneration, we investigated the temporal expression profile of Fmn2 after sciatic nerve crush injury, whereas PNI induced downregulation of *Fmn2* expression in DRGs. Complete *Fmn2* knockout ($Fmn2^{-/-}$) accelerated axon regeneration and function recovery after PNI. To further determine the specific role of Fmn2 in neurons, we knocked down *Fmn2* expression in DRG and motor neurons with a high neuronal tropism adeno-associated virus (AAV) serotype 2/9,[16,51–53] and the specificity of neuronal knockdown was verified by eGFP-directed fluorescence-activated cell sorting (FACS). Similar growth-promoting effects were observed in AAV2/9-*Fmn2*- short hairpin RNA (shRNA) mice. Mechanistically, Fmn2 knockdown increased the microtubule dynamics in growth cones of DRG neurons by enhancing the displacement rate of microtubule end-binding protein 3 (EB3) comets. In AAV2/9-*Fmn2*-shRNA mice, tubulin deacetylation in distal regenerating axons was increased substantially together with the upregulation of phosphorylated form of HDAC5. By inhibiting HDAC5 with a selective HDAC4/5 inhibitor LMK-235 or neuronal *Hdac5* knockdown (AAV2/9-*Hdac5*-shRNA), the promoting effect of neuronal *Fmn2* knockdown on axon regeneration was completely eliminated. Finally, we performed a small-molecule bioinformatics analysis of $Fmn2^{-/-}$ and identified a US Food and Drug Administration (FDA)-approved small-molecule metaxalone that promoted *in vitro/in vivo* axon regeneration and function recovery. Metaxalone treatment delayed by 24 h post-injury still maintained full therapeutic effect on function recovery. As a proof of concept, this study provides a potential small-molecule-based strategy for PNI.

RESULTS

LDIR enhances the intrinsic growth capacity of injured neurons and functional recovery

Ionizing radiation such as α-particle and X-ray is commonly used in biological studies and medical applications. LDIR exerts neuroprotective effects in mouse models of Alzheimer's disease, Parkinson's disease, glaucoma, diabetic neuropathy, and retinitis pigmentosa.[43,54] In a recent study, the beneficial effect of LDIR was observed in rats by performing local irradiation on the sciatic nerve directly, but the underlying mechanism remains unknown.[45] We, therefore, hypothesize that LDIR not only promotes the overall physiological functioning of living organisms but also enhances intrinsic growth capacity of injured DRG neurons since DRGs directly supply the sciatic nerve. We first demonstrated that 20 mGy α-particle induced a 39.9% and

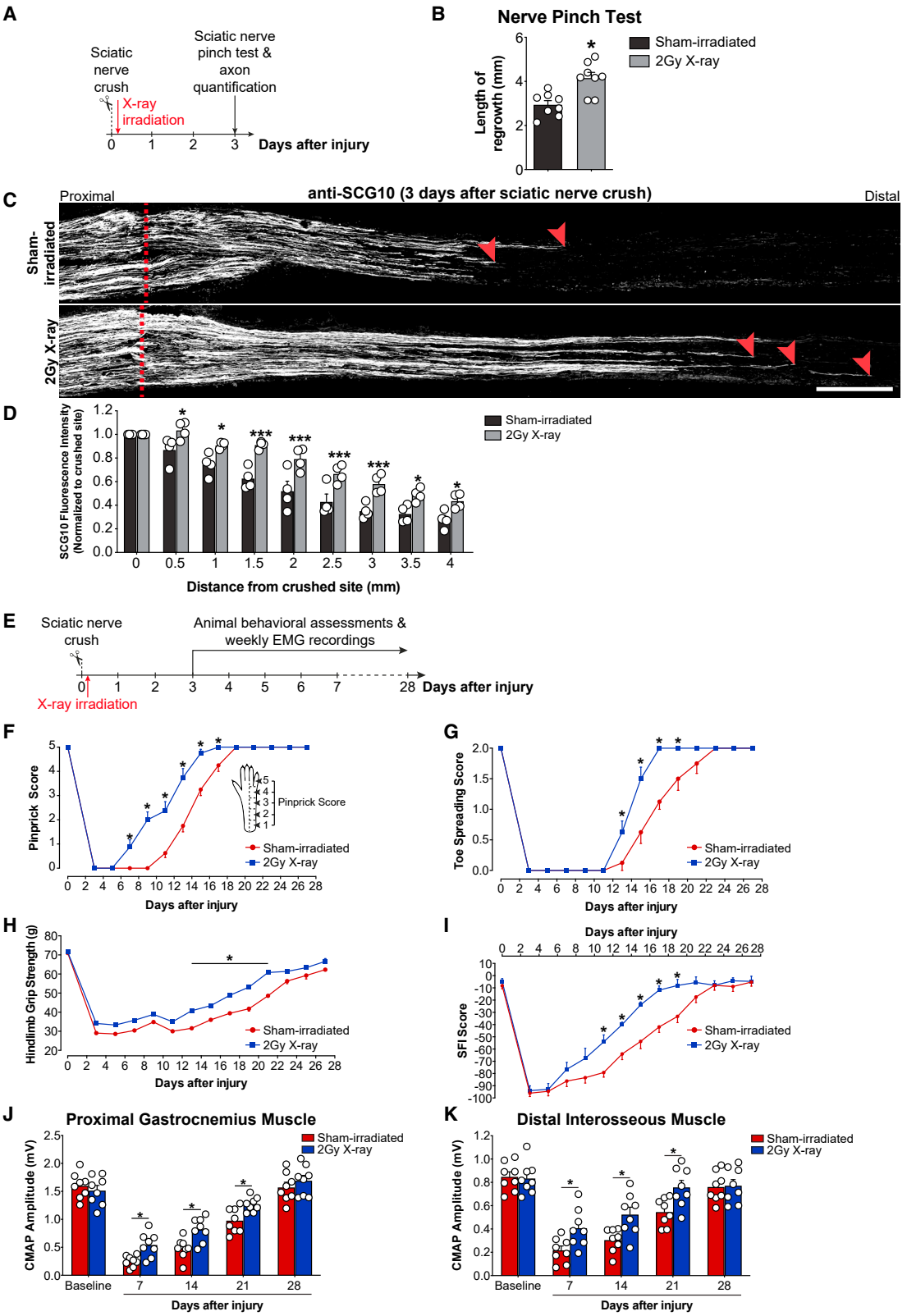

(legend on next page)

35.5% increase in total neurite outgrowth and average longest neurite length of DRG neurons, respectively (Figures S1A and S1B). Furthermore, we observed a robust neurite outgrowth after LD X-ray irradiation, which has a higher penetrating power than α-particle, with its maximal promoting effect on total neurite outgrowth (89.0%) and longest neurite length at 150 mGy (66.7%) (Figures S1C and S1D). α-particle and X-ray irradiation showed no adverse effects on cell survival as measured with the WST-1 cell cytotoxicity assay (Figure S1E).

We then extended these *in vitro* findings to whole-body X-ray irradiation (Figure S1F) and investigated whether LD X-ray irradiation could increase the intrinsic growth capacity of axotomized neurons in DRG explant cultures. Notably, whole-body X-ray irradiation at 2 Gy showed a dramatic increase of 54.8% and 68.4% in total neurite outgrowth and longest neurite length, respectively (Figure S1G). We validated our *ex vivo* DRG explant results with a sciatic nerve pinch test to measure the rate of *in vivo* axon regeneration (Figure 1A). We observed a 41.2% increase in axon regeneration in mice exposed to a single X-ray irradiation at 2 Gy immediately after crush when compared with sham-irradiated mice (Figure 1B). The nerve pinch test results were validated by immunostaining for superior cervical ganglion 10 (SCG10), which is preferentially expressed in regenerating sensory axons. Regeneration index was calculated by normalizing the average SCG10 immunoreactivity in the longitudinal section of sciatic nerve measured at different distal distances to the SCG10 immunoreactivity at the crush site, indicating the length and the number of axons have regenerated past the crush site (Figure 1C).[16,53,55] The regeneration index at the region over 4 mm from the injury site was significantly higher in nerves treated with 2 Gy X-ray irradiation compared with sham-irradiated control 3 days after sciatic nerve crush, demonstrating that X-ray irradiation accelerates axon regeneration in the injured sciatic nerves of mice (Figure 1D).

To examine if this increase in intrinsic growth capacity could promote *in vivo* functional recovery for an extend period of time (28 days), adult mice were exposed to a single dose of X-ray irradiation at 2 Gy immediately after crush. Sensory and motor function recovery were monitored for 28 days by a battery of animal behavioral tests (Figure 1E).[3,4,8,9,56,57] X-ray-irradiated mice demonstrated an early initial pinprick sensory response, which was 4 days earlier than the sham-irradiated mice (Figure 1F). For motor function recovery, X-ray-irradiated mice regained full toe-spreading reflex 6 days earlier than sham-irradiated mice (Figure 1G) and showed a faster recovery of hindlimb grip strength than the sham-irradiated mice (Figure 1H). Gait analysis of walking track by sciatic function index (SFI) demonstrated that at days 11–19 post-injury, the motor recovery of X-ray-irradiated mice was significantly higher than the sham-irradiated mice (Figure 1I). The accelerated motor function recovery was validated by electromyography (EMG) recording[4,8,9,56,57] showing significant increase in compound muscle action potential (CMAP) amplitude in hindlimb proximal (gastrocnemius) and distal plantar muscles (interosseous) of X-ray-irradiated mice at days 7, 14, and 21 post-injury, when compared with the sham-irradiated controls (Figures 1J and 1K).

LDIR induces hypermethylation of Fmn2 promoter, and *Fmn2* expression is downregulated in DRGs in response to PNI

To delineate the LDIR-induced intrinsic growth program, we performed a genome-wide CpG methylation profiling by reduced representation bisulfite sequencing (RRBS) of purified DRG neurons after treating with optimal doses of α-particle (20 mGy) or X-ray irradiation (150 mGy). Global DNA methylation was found not to be affected by LDIR. The methylation level of CpG sites of either α-particle- or X-ray-irradiated DRG neurons was comparable to their sham-irradiated controls: ∼60% CpG sites were weakly methylated (0%–10% methylated), whereas ∼28% CpG sites were highly methylated (>70% methylated) (Figure S2A). The absence of global DNA methylation in LDIR-treated DRG neurons suggested no changes in the gene expression of methylation machinery such as the DNA methyltransferases (*Dnmt1*, *Dnmt3a*, *Dnmt3b*, and *Gadd45b*), as confirmed by qPCR analysis (Figure S2B). We did not detect any significant differences in gene expression levels of key RAGs in DRG neurons after treated with either α-particle- or X-ray-irradiation (Figure S2C).

We then explore the possibility of DNA methylation at promoter regions that could be correlated with the transcriptional activation/inhibition of a corresponding gene after LDIR. We found that 206 genes were differentially methylated at the CpG sites of promoter regions between α-particle-irradiated and sham-irradiated neurons (differential methylation difference >20%).[58] Of these differentially methylated genes, 117 genes were hypermethylated and 89 genes were hypomethylated (Figure S2D). In the X-ray-irradiated neurons, CpG island promoter of 80 genes was hypermethylated, and 44 genes were hypomethylated (Figure S2E). Of these differentially methylated genes, 7 genes were uniquely expressed in both α-particle and X-ray-irradiated DRGs that shared similar overall percentages of CpG island promoter hypermethylation or hypomethylation (Table S1). Correlation analysis of mRNA expression levels and DNA methylation levels of these 7 genes was performed. Notably, we observed a

Figure 1. LDIR promotes robust axon regeneration and function recovery after PNI

(A) LDIR treatment paradigm for sciatic nerve pinch test.

(B) LD-X-ray irradiation accelerated axon regeneration (n = 8 per group). Each dot represents axonal regrowth per mouse.

(C) Representative longitudinal sections of sciatic nerve immunostained with anti-SCG10 antibody. Dotted line: site of injury. Arrowhead: distal regenerating axons. Scale bars, 500 μm.

(D) Regeneration index was measured as SCG10 immunoreactivity normalized to the crush site (n = 4 per group). Each dot represents normalized SCG10 immunoreactivity per mouse.

(E) Treatment paradigm for sciatic nerve injury.

(F–I) X-ray-irradiated mice exhibited substantial promoting effects on sensory (F) and motor (G–I) function recovery (n = 8 per group).

(J and K) Electromyography recording showing significant increase in CMAP amplitude in proximal gastrocnemius muscle (J) and distal interosseous muscle (K) of X-ray-irradiated mice after injury (n = 8 per group). Each dot represents average CMAP amplitude per mouse. Mean ± SEM. *$p < 0.05$, ***$p < 0.001$; Student's t test in (B), two-way ANOVA with post hoc Bonferroni test for (D), two-way ANOVA with repeated measures followed by post hoc Bonferroni's test for (F)–(K).

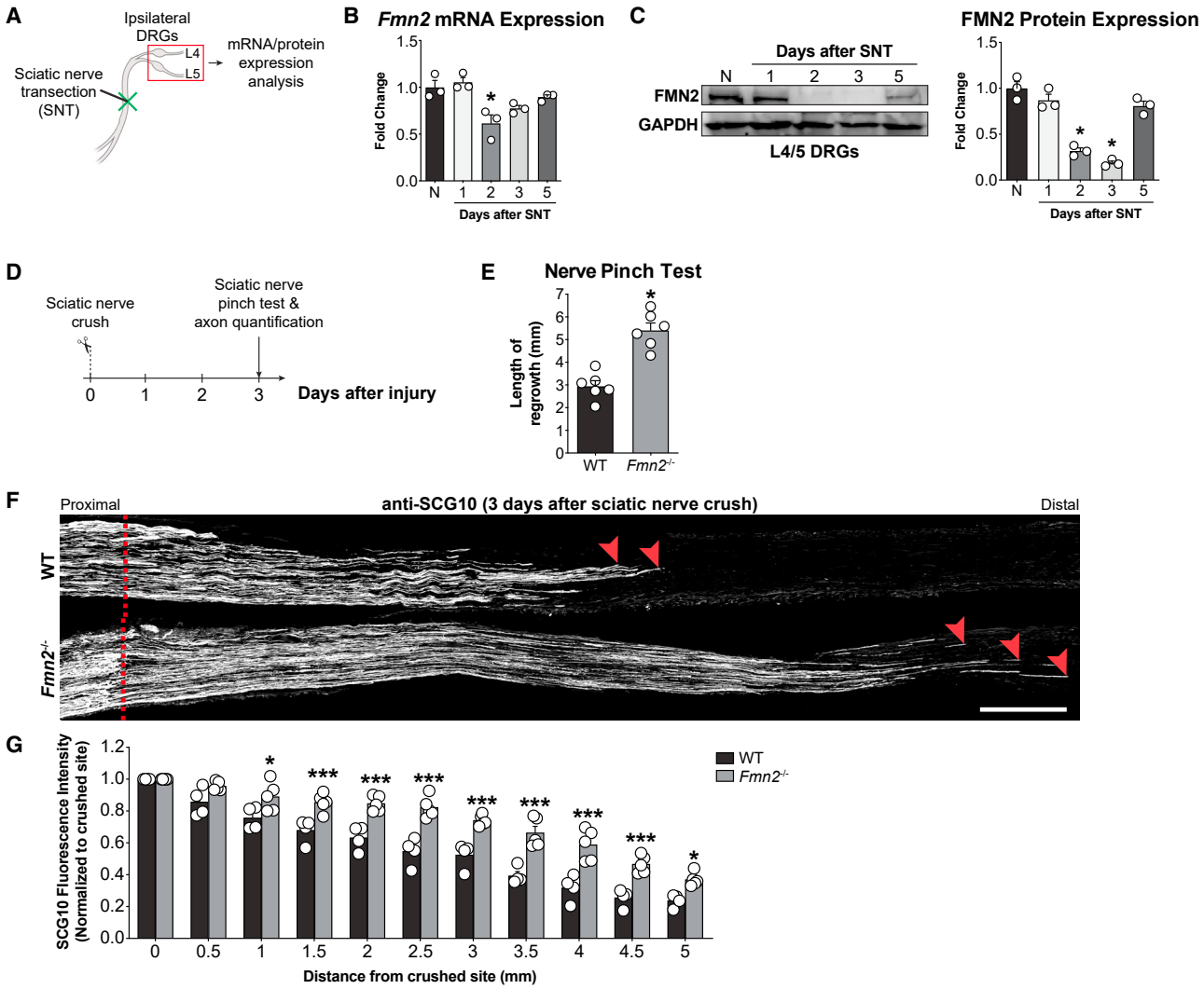

Figure 2. Fmn2 is a negative regulator of axon regeneration in mice

(A) Sciatic nerve transection was performed, and ipsilateral L4/5 DRGs were harvested.

(B and C) Fmn2 expression was significantly downregulated after sciatic nerve injury at both mRNA (B) and protein (C) levels (n = 3 per time point). Each dot represents one pooled mRNA or protein sample of L4/5 DRGs from 3 mice. FMN2 expression was normalized to GAPDH.

(D) Paradigm for sciatic nerve pinch test.

(E) The distal extent of sensory axonal regrowth was markedly increased in *Fmn2*$^{-/-}$ mice (n = 6 per group). Each dot represents axonal regrowth per mouse.

(F) *Fmn2*$^{-/-}$ mice exhibited an increased number in SCG10-positive regenerating axons distal to the crush site. Dotted line: site of injury. Arrowhead: distal regenerating axons. Scale bars, 500 μm.

(G) Regeneration index was calculated (n = 4–5 per group). Each dot represents normalized SCG10 immunoreactivity per mouse. Mean ± SEM. *p < 0.05, ***p < 0.001; one-way ANOVA with post hoc Bonferroni test for (B and C), Student's t test for (E), and two-way ANOVA with post hoc Bonferroni test for (G). SNT, sciatic nerve transection; N, naive control mice; WT, wild type.

significant downregulation (hypermethylation) of *Fmn2* mRNA expression in the α-particle-irradiated (32%) and X-ray-irradiated (22%) DRG neurons in cultures, when compared with sham-irradiated controls. The gene expression of the remaining 6 genes was largely unaffected regardless of their hypermethylation/hypomethylation status (Figure S3). In fact, the actual gene expression of hypermethylated/hypomethylated genes can be unaffected or even upregulated/downregulated in some cases.[59]

Thousands of genes are differentially expressed (DE) after PNI, which orchestrate the intrinsic growth program to prime injured neurons into an actively growing state for successful axon regeneration.[3,60] To verify the involvement of Fmn2 in the intrinsic growth program, we examined mRNA and protein expression of Fmn2 in injured lumbar 4 and 5 (L4/5) DRGs, which directly supply the sciatic nerve (Figure 2A). We detected a significant downregulation of Fmn2 mRNA (38.6%) (Figure 2B) and protein expression (68.2%–81.6%) (Figure 2C) in DRGs 2–3 days following sciatic nerve injury. These results confirm the injury-induced Fmn2 downregulation in injured DRGs and suggest Fmn2 as a potential target gene for axon regeneration.

Genetic ablation of Fmn2 enhances intrinsic growth capacity of injured neurons and accelerates function recovery after PNI

We then extended these findings to examine the intrinsic growth capacity of axotomized and preconditioned (induced maximal growth capacity) DRG neurons from *Fmn2* complete knockout (*Fmn2*$^{-/-}$) mice, which have been used extensively to study the roles of FMN2 in oocyte development.[61–65] *Fmn2*$^{-/-}$ mice are viable with no major defect except poor fertility in female and show no gross or histological brain differences as compared with wild-type (WT) mice.[64] Primary DRG neurons derived from *Fmn2*$^{-/-}$ mice exhibited significantly more neurite outgrowth and longer neurite length when compared with the WT mice. Total neurite outgrowth and the average longest neurite length in *Fmn2*$^{-/-}$ DRG neurons were increased by 71.5% and 82.1%, respectively (Figure S4A). We demonstrated that a preconditioning lesion to the sciatic nerve increased neurite outgrowth of DRG explant from WT mice, whereas *Fmn2* ablation significantly potentiated the preconditioning effect in neurite outgrowth by 81.8% (total neurite outgrowth) and 78.4% (average longest neurite) (Figure S4B). Next, we performed sciatic nerve crush injury on *Fmn2*$^{-/-}$ mice and assessed the extent of axonal regrowth by sciatic nerve pinch test 3 days after injury (Figure 2D). Consistent with our *in vitro* results, *Fmn2* ablation markedly enhanced the distal extent of axonal regrowth by 83.5% (5.4 ± 0.3 mm in *Fmn2*$^{-/-}$ mice versus 2.9 ± 0.2 mm in WT mice) (Figure 2E). We found that *Fmn2*$^{-/-}$ mice exhibited longer SCG10-positive regenerating axons in the injured sciatic nerves compared with the WT control nerves (Figure 2F). Significant SCG10 immunoreactivity was observed even in the far distal region of the injured nerves at 5 mm away from the injury site (Figure 2G).

To examine if increased intrinsic growth capacity and *in vivo* axon regeneration in *Fmn2*$^{-/-}$ mice contribute to the acceleration of function recovery after PNI, we assessed sensory and motor function recovery by an exhaustive list of animal behavior and electrophysiology tests. In *Fmn2*$^{-/-}$ mice, the initial return of sensory function measured by pinprick assay was significantly earlier than the WT mice by 4 days. *Fmn2*$^{-/-}$ mice regained full sensory function at day 17, which was 2 days earlier than the WT mice (Figure S5A). For motor function recovery, *Fmn2*$^{-/-}$ mice fully regained toe-spreading reflexes at day 19 post-injury, 4 days earlier than the WT mice (Figure S5B). Accelerated motor functional recovery was confirmed by grip strength tests in *Fmn2*$^{-/-}$ mice, which exhibited significantly higher grip strength than controls from days 7 to 23 (Figure S5C). Gait movement assessed by SFI showed significant motor functional recovery in *Fmn2*$^{-/-}$ mice from days 9 to 17, compared with WT controls (Figure S5D). The promoting effect observed by behavior tests was validated by muscle EMG recording showing increased CMAP amplitudes in proximal (gastrocnemius: 1 week, 86.6%; 2 weeks, 56.4%; and 3 weeks, 42.0%) (Figure S5E) and distal plantar muscle (interosseous: 1 week, 51.9%; 2 weeks, 61.6%; and 3 weeks, 28.0%) (Figure S5F) of *Fmn2*$^{-/-}$ mice when compared with WT controls after injury.

Ablation of FMN2 expression in DRGs with a high neuronal tropism AAV serotype promotes *in vivo* axon regeneration and function recovery after PNI

Fmn2 is almost exclusively expressed in the nervous system, including the brain, spinal cord, and DRG, in mice during development[63]; however, little is known about its mechanistic roles in axon regeneration after PNI. To overcome limitations of the global *Fmn2* knockout mice, we knocked down neuronal Fmn2 expression by expressing a shRNA directed against *Fmn2* mRNA using a recombinant AAV (AAV2/9-*Fmn2*-shRNA) injected into the sciatic nerves.[51,52,66,67] Among the commonly used AAV serotypes, AAV2/9 showed a superior ability to transduce neurons in DRGs following peripheral routes of delivery.[51,52] Mice injected with AAV2/9-scrambled (scr) shRNA-eGFP showed a high level of transduction of lumbar DRG and motor neurons at 2 weeks after sciatic nerve injection. Indeed, the eGFP signal was observed in 72% of total βIII-tubulin-positive neurons (Figure S6A) and in 75% of ChAT-positive neurons (Figure S6B). By contrast, eGFP signal was not found in SOX10-positive Schwann cells (Figure S6C). To examine if AAV2/9 targeted gene delivery to non-neuronal cell populations in the sciatic nerves near to the AAV2/9 injection sites, we examined co-localization of eGFP and SOX10/CD68 immunofluorescent signals in the sciatic nerves and found that virtually no eGFP immunofluorescence co-localized with SOX10-positive Schwann cells (Figure S6D) or with CD68-positive macrophages (Figure S6E), indicating that AAV2/9 preferentially transduces neurons but not non-neuronal cells. We further analyzed the population of transduced cells by performing flow cytometry on L4/5 DRGs 2 weeks after AAV2/9 injection into the sciatic nerve (Figures S7A and S7B). Our western blot analysis demonstrated that NeuN (pan-neuronal marker), but not the glial cell makers such as SOX10 (Schwan cells) and ionized calcium-binding adapter molecule-1 (IBA-1) (microglia), was strongly expressed in the sorted eGFP-positive cells from AAV2/9-*scr*-shRNA-treated or AAV2/9-*Fmn2*-shRNA-treated mice. In those sorted eGFP-positive neurons collected from DRGs of AAV2/9-Fmn2-shRNA-treated mice, we detected high knockdown efficiency of Fmn2 protein expression (69.2%) (Figure S7C). Additionally, Fmn2 expression in the ventral horn of the spinal cord from AAV2/9-*Fmn2*-shRNA-treated mice showed high knockdown efficiency (55%), when compared with AAV2/9-*scr*-shRNA-treated mice (Figure S7D). To confirm the western blot results, we performed immunohistologic studies on spinal cord to visualize the knockdown efficiency of Fmn2 in motor neurons. In AAV2/9-*Fmn2*-shRNA-treated mice, GFP expression was highly abundant in ChAT-positive motor neurons (white arrowheads), whereas the Fmn2 expression was greatly reduced to undetectable expression levels. By contrast, the expression of Fmn2 in untransduced ChAT-positive motor neurons remained at a high level (yellow arrowheads) (Figure S7E). These results unequivocally demonstrate the high neuronal tropism of AAV serotype 2/9 in our studies and the specificity of *Fmn2* knockdown in neurons.

To determine the effect of neuronal *Fmn2* knockdown on *in vivo* axon regeneration and function recovery, we injected AAV2/9-*Fmn2*-shRNA into the sciatic nerves (Figure S8A). Similarly, it showed a significantly high knockdown efficiency of *Fmn2* (69.2%) in L4/5 DRGs at 2 weeks after injection (Figure S8B). We observed a significant increase in axon regeneration in AAV2/9-*Fmn2*-shRNA mice (5.3 ± 0.3 mm) (Figure S8C). The number of SCG10-positive regenerating axons 5 mm distal to the crush site was significantly higher in AAV2/9-*Fmn2*-shRNA

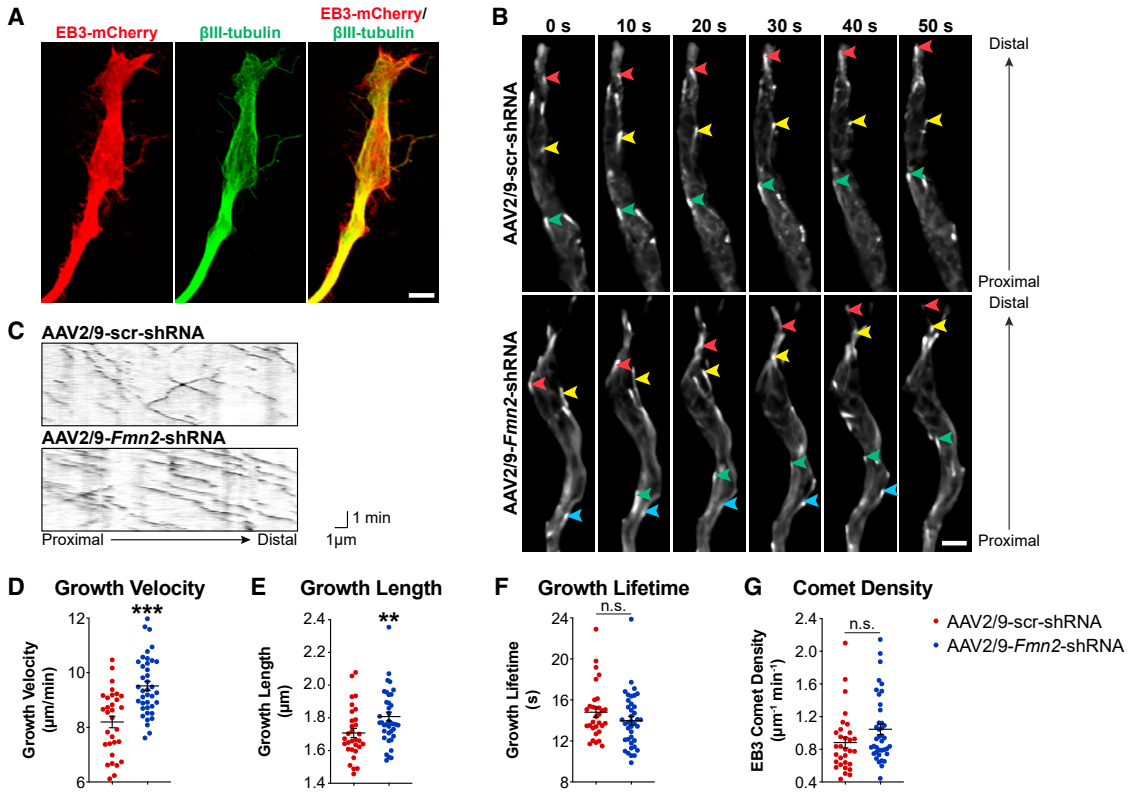

Figure 3. Gene silencing of neuronal *Fmn2* increases microtubule dynamics in cultured DRG neurons

(A) Representative photomicrographs demonstrated the growth cones of DRG neurons expressing microtubule plus-end marker EB3-mCherry (red) and neuronal markers βIII-tubulin (green). Scale bars, 5 μm.

(B) Series of time-lapse images indicating the movement of EB3 comets. Arrowheads with the same color indicated the movement of individual EB3 comet across time. Scale bars, 2 μm.

(C) Representative kymographs of EB3 comet motion. The movement of individual EB3 comets (black lines) was recorded for 5 min (1 frame/2 s).

(D–G) The motion of each EB3 comet was automatically traced, and microtubule dynamics was assessed using plusTipTracker software. *Fmn2* knockdown resulted in a substantial increase in the average microtubule growth velocity (D) and length (E) of EB3 comets, whereas the microtubule growth lifetime (F) and EB3 comet density (G) remained unchanged after gene silencing of *Fmn2*. Each dot in (D)–(G) represents the average microtubule growth velocity/length/lifetime/comet density of EB3 comets per growth cone. N = 31 (AAV2/9-scr-shRNA-treated neurons) and 39 (AAV2/9-*Fmn2*-shRNA-treated neurons) growth cones from 3 independent experiments. Mean ± SEM. **p < 0.01, ***p < 0.001; Mann-Whitney U test for (D)–(G). n.s., not significant.

mice than that in the AAV2/9-scr-shRNA control mice (Figure S8D), suggesting that the axonal regrowth-promoting effects of *Fmn2* knockout are primarily mediated by neurons. As expected, our behavioral and electrophysiology studies (Figure S8E) demonstrated that accelerated axon regeneration in AAV2/9-*Fmn2*-shRNA mice promoted sensory (Figure S8F) and motor function recovery (Figures S8G–S8I) and facilitated the formation of functional neuromuscular junction following sciatic nerve crush (Figures S8J and S8K).

The mechanistical roles of Fmn2 in microtubule dynamics and post-translational modification of tubulin

Microtubules are highly dynamic structures that undergo continuous assembly (polymerization) and disassembly (depolymerization). The dynamic growing plus end of microtubules act as "sensors" of cellular microenvironment, which allow the rapid reorganization of the cytoskeleton for successful axon regeneration.[68] Microtubule dynamics can also be affected by the post-translational modifications such as tubulin acetylation and deacetylation.[31] We, therefore, first assayed microtubule dynamics quantitatively using high-resolution time-lapse confocal microscopy and fluorescently tagged microtubule EB3 in peripheral axons. To this end, we purified DRG neurons from adult mice and transduced the DRG neurons with AAV2/9-EB3-mCherry. 4 days upon transduction, the growth cones were categorized as both GFP-positive and EB3-positive during the live-cell imaging with the confirmation of βIII-tubulin immunoreactivity after fixation (Figure 3A) and a series of 5-min time-lapsing images (with a time interval of 2 s per frame) were captured. Microtubule dynamics were quantified by tracking the displacement of EB3 comets (and therefore growing microtubules) at the microtubules plus ends in sequential frames of time-lapsing images (Figure 3B; Video S1). Kymographs analysis of EB3-mCherry signals exhibited EB3-mCherry comet trajectories with increasing comet speed at the distal ends of *Fmn2*-deficient DRG neurons (Figure 3C). The movement of these EB3 comets can be used to determine microtubule dynamics quantitatively by using an automated MATLAB-based software plusTipTracker.[69,70] Compared

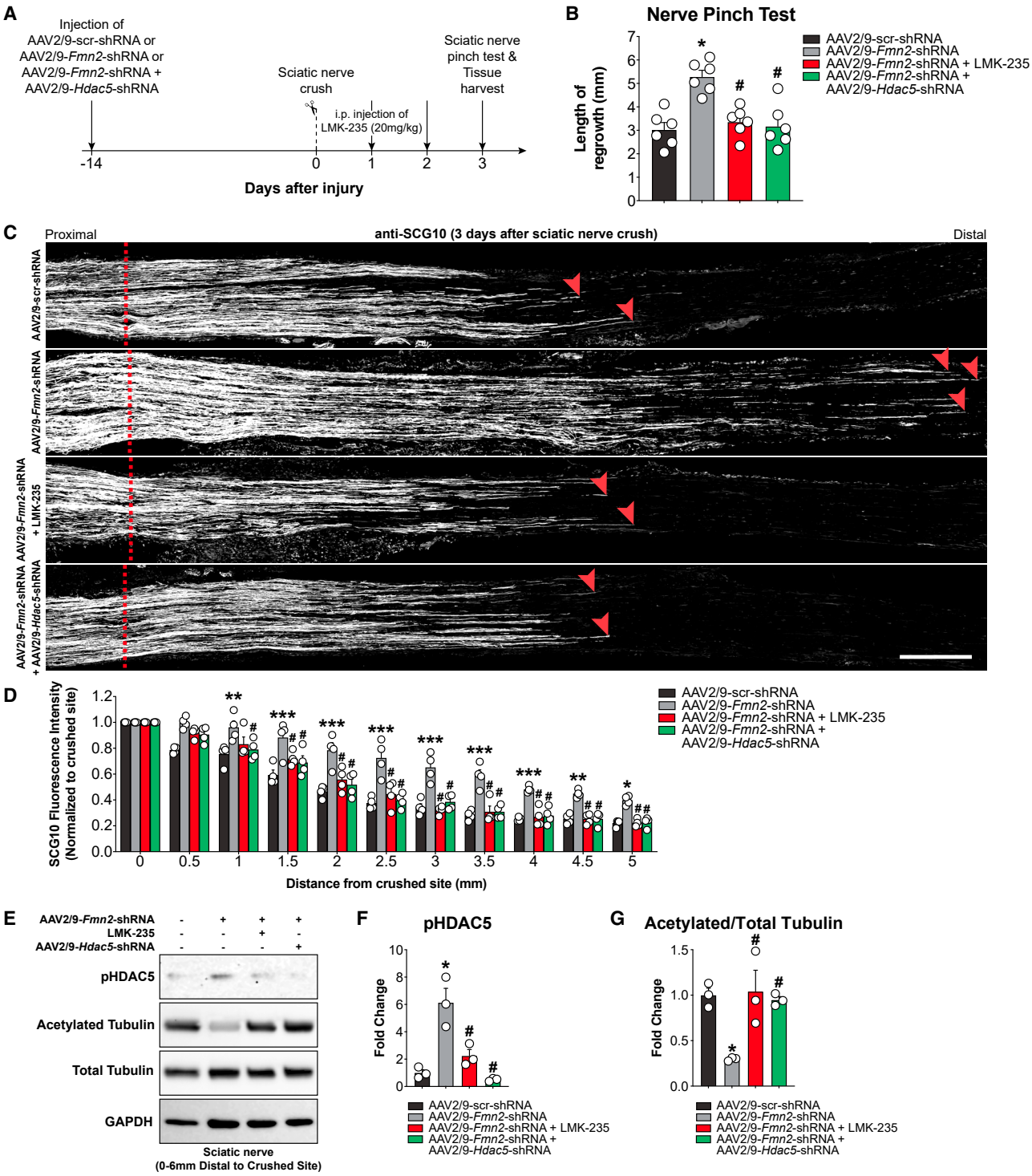

Figure 4. Fmn2 expression is a critical determinant of α-tubulin deacetylation in the regenerating axons in a HDAC5-dependent manner

(A) AAV2/9-*Fmn2*-shRNA, AAV2/9-*Hdac5*-shRNA, or AAV2/9-scrambled (scr)-shRNA were injected directly into the sciatic nerves. LMK-235 was injected intraperitoneally immediately after crush for 3 consecutive days.

(B) The distal extent of axonal regrowth was markedly increased in AAV2/9-*Fmn2*-shRNA mice. LMK-235 or AAV2/9-*Hdac5*-shRNA treatment reduced the growth-promoting effects induced by *Fmn2* deletion (n = 6 per group). Each dot represents axonal regrowth per mouse.

(C) Representative SCG10 immunostaining of sciatic nerves. Dotted line: site of injury. Arrowhead: distal regenerating axons. Scale bars, 500 μm.

(D) Regenerative index was calculated (n = 4 per group). Each dot represents normalized SCG10 immunoreactivity per mouse.

(legend continued on next page)

with AAV2/9-scr-shRNA control DRG neurons, the speed of microtubule polymerization (growth velocity) was markedly increased by 16.1% in *Fmn2*-deficient DRG neurons, indicating that the *Fmn2*-deficient microtubules grew significantly faster than the control microtubules (8.20 ± 0.21 μm/min versus 9.52 ± 0.17 μm/min). *Fmn2*-deficient DRG neurons also displayed a significant increase in microtubule growth length, which represented the total displacement of EB3 comets before they were paused or catastrophe (1.71 ± 0.03 μm in AAV2/9-scr-shRNA neurons versus 1.81 ± 0.03 μm in AAV2/9-*Fmn2*-shRNA neurons) (Figure 3E). *Fmn2* knockdown did not affect the duration of microtubule polymerization (growth lifetime) (Figure 3F) and the density of EB3 comets in the growth cones (Figure 3G). Our data suggest that Fmn2 knockdown increases the microtubule dynamics in growth cones, which is consistent with previous studies on the role of Fmn2 as a regulator of growth cone dynamics in cultured chick spinal commissural neurons and zebrafish.[71]

Formin protein, including Fmn2, contains highly conserved formin homology 1 (FH1) and FH2 domains at the C terminus. A growing body of work suggests that FH1 and FH2 domains modulate microtubule stability and dynamic[62,72–75] by inducing α-tubulin acetylation.[75] Histone deacetylase 5 (HDAC5) phosphorylation-medicated α-tubulin deacetylation is crucial for axon regeneration.[23,76] For instance, sciatic nerve injury induces phosphorylation of HDAC5 in injured axons *in vivo*, and it has been shown that pHDAC5 catalyzes deacetylation of α-tubulin in axons to promote axon regeneration.[23] To examine the mechanistic roles of neuronal Fmn2 expression in axon regeneration and, more specifically, whether HDAC5 is responsible for the *Fmn2*-deletion-induced growth-promoting effect, we injected LMK-235 intraperitoneally, a selective inhibitor of HDAC4 and HDAC5, which has been reported to preferentially inhibit HDAC5 activity at low-dose exposure[77–79] immediately following sciatic nerve crush and assessed *in vivo* axon regeneration by nerve pinch test (Figure 4A). At 3 days after sciatic nerve injury, LMK-235 completely eliminated the axon regrowth-promoting effect in AAV2/9-*Fmn2*-shRNA mice to a level comparable to that of AAV2/9-scr-shRNA control mice. To rule out the possibility of any non-specific inhibition of HDAC4 even at low concentration of LMK-235, we knocked down HDAC5 expression by expressing a shRNA directed against *Hdac5* mRNA using AAV2/9 (AAV2/9-*Hdac5*-shRNA) injected into the sciatic nerves, resulting in a similar reduction in the rate of distal axon regeneration and the number of SCG10-positive regenerating axons at 3 days after injury (Figures 4B–4D). Consistent with observations in AAV2/9-*Fmn2*-shRNA knockdown experiments, AAV2/9-*Hdac5*-shRNA also significantly reduced HDAC5 protein expression in L4/5 DRGs by 57.8% (Figure S9). Next, we examined pHDAC5 and acetylated tubulin protein expression in 0–6 mm sciatic nerve segments distal to the crush injury site in the AAV2/9-scr-shRNA and AAV2/9-*Fmn2*-shRNA mice at 3 days after the injury by western blot analysis (Figure 4E). In the 0–6 mm sciatic nerve segments distal to the crush site where active axon regeneration is taking place in the AAV2/9-*Fmn2*-shRNA mice according to our nerve pinch test results in Figure 4B, densitometry of the resulting bands indicated a 5.13-fold increase in pHDAC5 protein at day 3 after injury (Figure 4F), which appeared to correlate with the decreased acetylated tubulin expression (70.3%) in AAV2/9-*Fmn2*-shRNA mice (Figure 4G). Similarly, either pharmaceutical blockade of HDAC5 by LMK-235 (70%) or gene silencing of HDAC5 using AAV2/9-*Hdac5*-shRNA (77%) substantially reduced the protein expression of pHDAC5, leading to increased acetylated tubulin expression in sciatic nerves of AAV2/9-*Fmn2*-shRNA mice at 3 days after injury (Figures 4E–4G).

Small-molecule bioinformatics analysis of *Fmn2*$^{-/-}$ gene expression signature and the identification of a therapeutic small-molecule metaxalone

Injury of axons in the PNS induces intrinsic growth capacity of neurons and transcriptional changes in gene expression that promote axon regeneration.[1–8] We, therefore, reasoned that if we could identify bioactive small molecules associated with the gene regulatory network of *Fmn2* deletion, switching on the intrinsic growth capacity of injured neurons would result in accelerated *in vivo* axon regeneration and recovery of function. To achieve this, we performed a whole transcriptome analysis and small-molecule bioinformatics analysis on L4/5 DRGs[8,60] from *Fmn2*$^{-/-}$ and their aged-matched WT mice 5 days after PNI. Hierarchical clustering and principal component analysis showed a clear separation between contralateral and ipsilateral DRGs regardless of genotypic differences (Figures 5A and 5B). After injury, there were 563 and 636 genes DE in *Fmn2*$^{-/-}$ and WT DRGs, respectively. Of these DE genes, 397 genes were upregulated, and 21 genes were downregulated in both *Fmn2*$^{-/-}$ and WT injured DRGs (Figure 5C). Specifically, key RAGs such as *Atf3*, *Sprr1a*, *Jun*, *Stmn4*, *Fabp5*, *Hspb1*, *Sox11*, and *Gap43*[3,60,80] were highly upregulated to a similar extent in both *Fmn2*$^{-/-}$ and WT injured DRGs. *Fmn2* deletion did not affect the RAG expression after PNI (Figure S10A). A total of 145 genes (87 upregulated and 58 downregulated) were uniquely DE only in *Fmn2*$^{-/-}$ mice but not in the WT mice after injury (Figure 5D). We then performed gene set enrichment analysis (GSEA) to identify core gene regulatory network governing the enhanced regenerative capacity in *Fmn2*$^{-/-}$ mice. We observed significant enrichment in signaling pathways associated with inflammatory responses such as Janus kinase/signal transducers and activators of transcription (Jak/Stat) and chemokine/cytokine-related signaling pathways (Figure S10B; see Table S2 for a complete list of signaling pathways).

(E) At 3 days post-injury, representative immunoblots revealed the activation of HDAC5 phosphorylation in AAV2/9-*Fmn2*-shRNA mice. Both pharmaceutical blockade and knockdown of HDAC5 eliminated *Fmn2*-deletion-induced tubulin deacetylation.
(F) pHDAC5 expression was normalized to GAPDH.
(G) Acetylated tubulin expression was first normalized to total tubulin levels and then normalized to GAPDH. Each dot in (F) and (G) represents one pooled protein sample of segmented sciatic nerves (0–6 mm distal to the crush site) from 3 mice. Mean ± SEM. *$p < 0.05$ when compared with AAV2/9-scr-shRNA-treated control mice; #$p < 0.05$ when compared with AAV2/9-*Fmn2*-shRNA-treated mice; one-way ANOVA with post hoc Bonferroni test for (B), (E), and (F), and two-way ANOVA with post hoc Bonferroni test for (D).

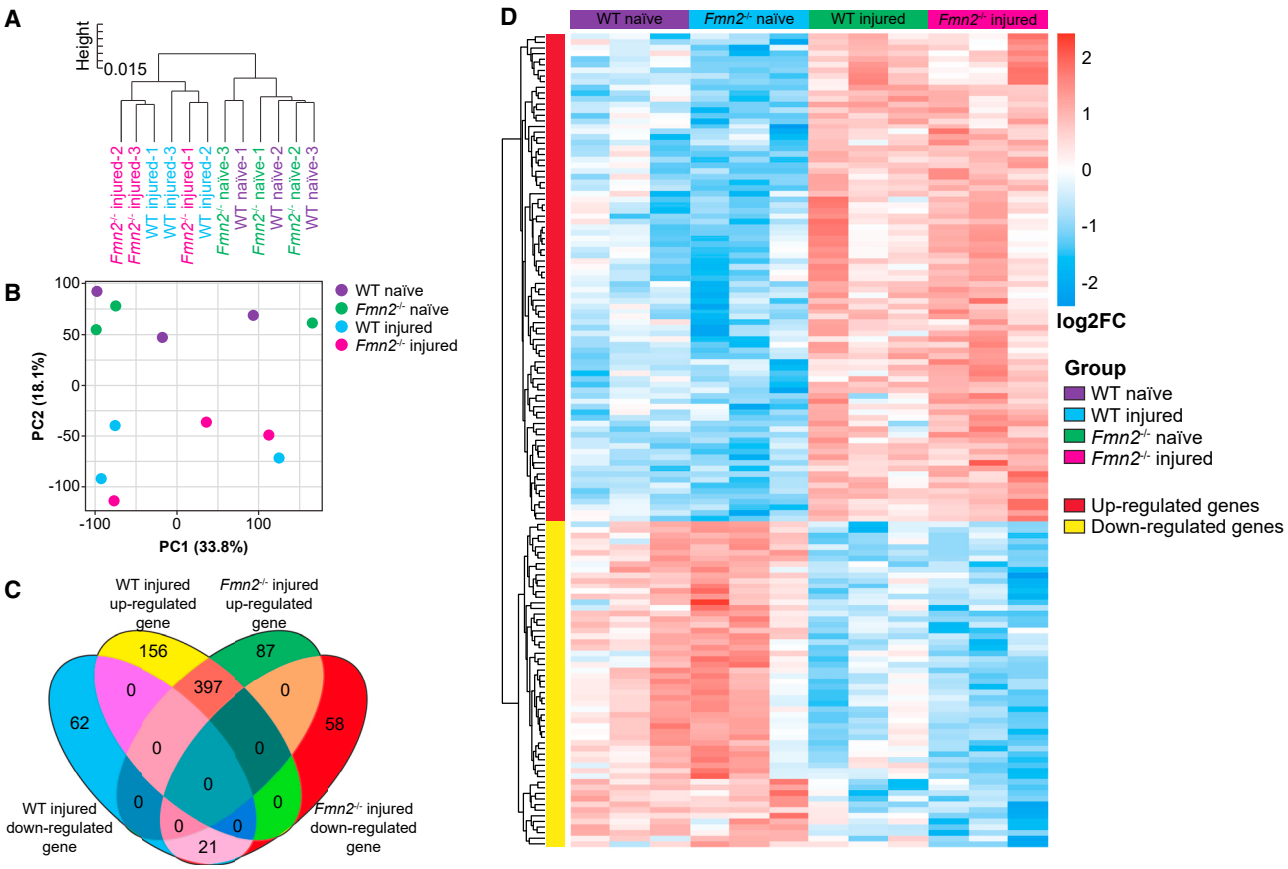

Figure 5. *Fmn2* deletion induces distinct transcriptional reprogramming as a unique gene signature for *in silico* screening of FDA-approved small molecules

L4/5 DRGs were used for RNA-seq whole transcriptome analysis 5 days after sciatic nerve injury.

(A and B) Hierarchical clustering and principal component analysis showed a clear separation between naive (uninjured) and injured DRG neurons regardless of genotypic differences.

(C) There were 87 upregulated and 58 downregulated genes that were differentially expressed in injured DRGs of *Fmn2*$^{-/-}$ mice only, which represented genotype-specific transcriptional regulation caused by genetic ablation of Fmn2.

(D) Heatmap of differentially expressed genes in which a total of 145 genes were differentially expressed in injured DRGs of *Fmn2*$^{-/-}$ mice only. Color intensity represents changes in $\log_2$FC from negative (light blue) to positive (dark brown).

Next, we utilized these 145 DE genes as gene expression signatures to query a public database, the Library of Integrated Network-Based Cellular Signatures (LINCS), and to match with gene expression profile derived from cell lines treated with small molecules based on connectivity and specificity scores (see STAR Methods for details).[60] We then selected four small molecules with connectivity score over 95 (score 100 being the highest) for experimental validation (Table S3) using sciatic nerve pinch test (Figure 6A). FDA-approved small-molecule metaxalone showed a marked increase of distal sensory axonal regrowth (4.82 ± 0.32 mm in metaxalone-treated mice versus 3.05 ± 0.16 mm in vehicle controls) 3 days after sciatic nerve crush injury (Figure 6B). In line with the pinch test results, we also observed a significant increase in the number of SCG10-positive regenerating axons in metaxalone-treated mice at 4.5 mm distal to the crush injury site when compared with vehicle controls (Figures 6C and 6D). As expected, metaxalone induced a substantial increase in protein expression of pHDAC5 (Figures 6E and 6F) associated with the reduction of tubulin acetylation (Figure 6G) in regenerating axons of sciatic nerves 3 days post-injury, demonstrating the recapitulation of growth-promoting mechanism induced by *Fmn2* deletion. To evaluate the direct effect of metaxalone on purified DRG neurons, we treated axotomized DRG neurons with increasing dose of metaxalone, and neurite outgrowth was increased almost linearly until reaching a plateau at 20 μM (Figure S11). Our results demonstrated that metaxalone could enhance the intrinsic growth capacity of injured DRG neurons directly.

Delayed metaxalone treatment promotes axon regeneration and function recovery

To simulate a clinically relevant situation where hours could elapse before any treatment is possibly available, we first evaluated the efficacy of post-injury treatment of metaxalone delayed by 24 h in promoting *in vivo* axon regeneration. We administered metaxalone 1 day after sciatic nerve crush injury. At 3 days post-injury, we

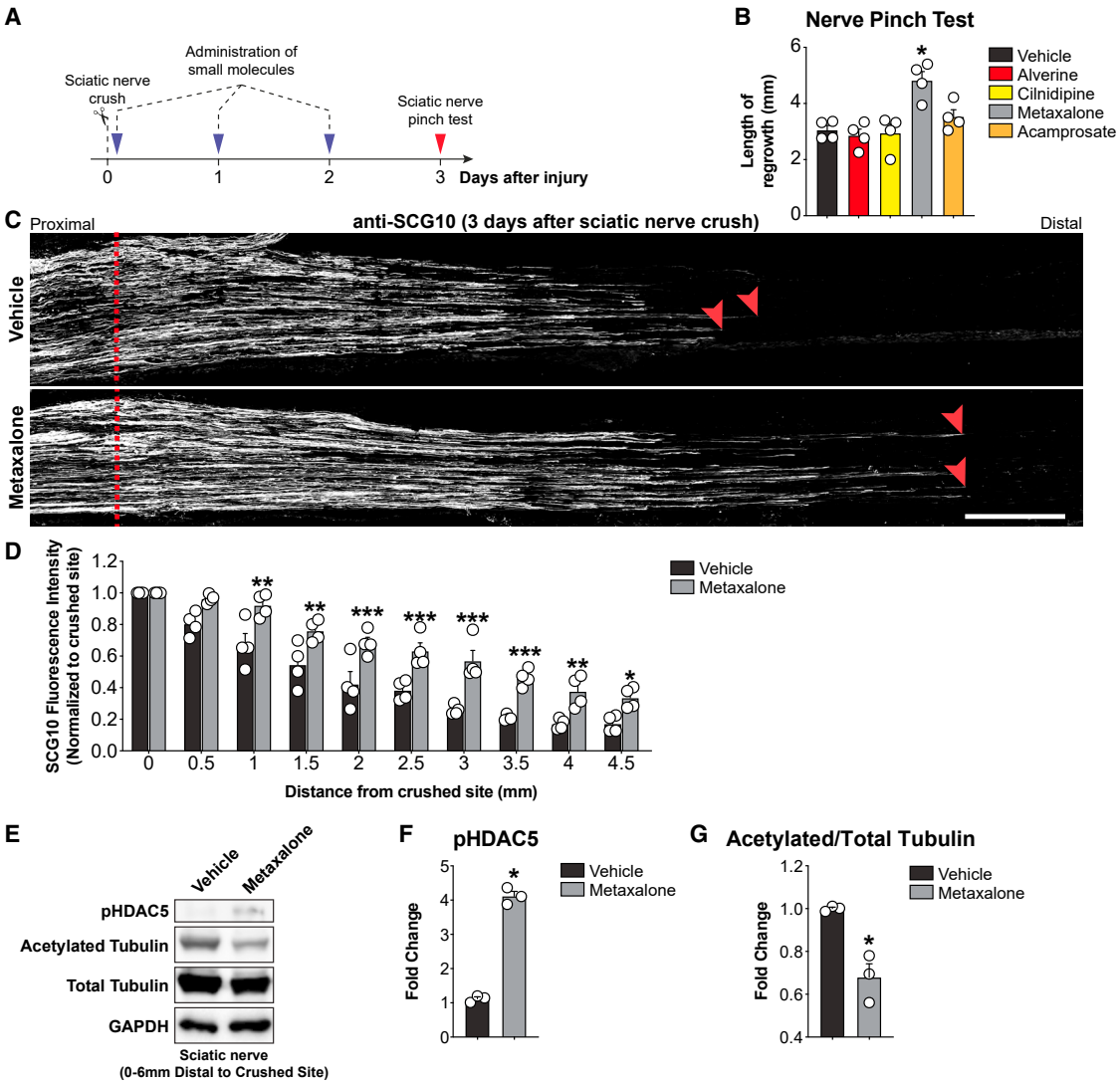

Figure 6. Clinical relevance FDA-approved metaxalone promotes *in vivo* axon regeneration after PNI

(A) Administration of four top-ranked small molecules directly onto the site of injury immediately after sciatic nerve crush (twice per day with an 8-h time interval).

(B) Metaxalone induced robust *in vivo* axon regeneration (n = 4 per group). Each dot represents axonal regrowth per mouse.

(C) Higher number of SCG10-positive distal regenerating axons in metaxalone-treated mice than controls. (n = 4 per group.) Dotted line: site of injury. Arrowhead: distal regenerating axons. Scale bars, 500 μm.

(D) Regeneration index was calculated. Each dot represents normalized SCG10 immunoreactivity per mouse.

(E) Metaxalone treatment induced robust activation of HDAC5 phosphorylation and reduced expression of acetylated tubulin in sciatic nerves at 3 days post-injury.

(F) pHDAC5 expression was normalized to GAPDH.

(G) Acetylated tubulin expression was first normalized to total tubulin levels, and then normalized to GAPDH. Each dot in (F) and (G) represents one pooled protein sample of segmented sciatic nerves (0–6 mm distal to the crush site) from 3 mice (n = 3 per group). Mean ± SEM. *p < 0.05, **p < 0.01, ***p < 0.001; one-way ANOVA with post hoc Bonferroni test for (B), two-way ANOVA with post hoc Bonferroni test for (D), Student's t test for (F) and (G).

performed nerve pinch test to assess the extent of axonal regrowth (Figure 7A). Similar to the mice treated with metaxalone immediately after injury (4.82 ± 0.32 mm) (see Figure 6B), accelerated axon regeneration was observed in the mice with delayed metaxalone treatment by 24 h (4.50 ± 0.25 mm) (Figure 7B). By examining the expression of SCG10, we found that the regeneration index at the region over 4.5 mm was similar in metaxalone-treated (0.34) (see Figure 6D) and delayed-metaxalone-treated (0.40) (Figures 7C and 7D) mice, indicating that metaxalone treatment delayed even by 24 h did not affect either the length or the number of regenerating axons past the crush site.

Finally, to further validate the therapeutic applicability of metaxalone in function recovery when treatment initiation was delayed until 24 h after PNI. Adult mice received 10 mg/kg of metaxalone[81] intraperitoneally once a day immediately after PNI for 21 consecutive days or delaying daily metaxalone treatment to 24 h post-injury for 20 consecutive days (Figure 7E). Metaxalone-treated and delayed-metaxalone-treated mice showed initial response

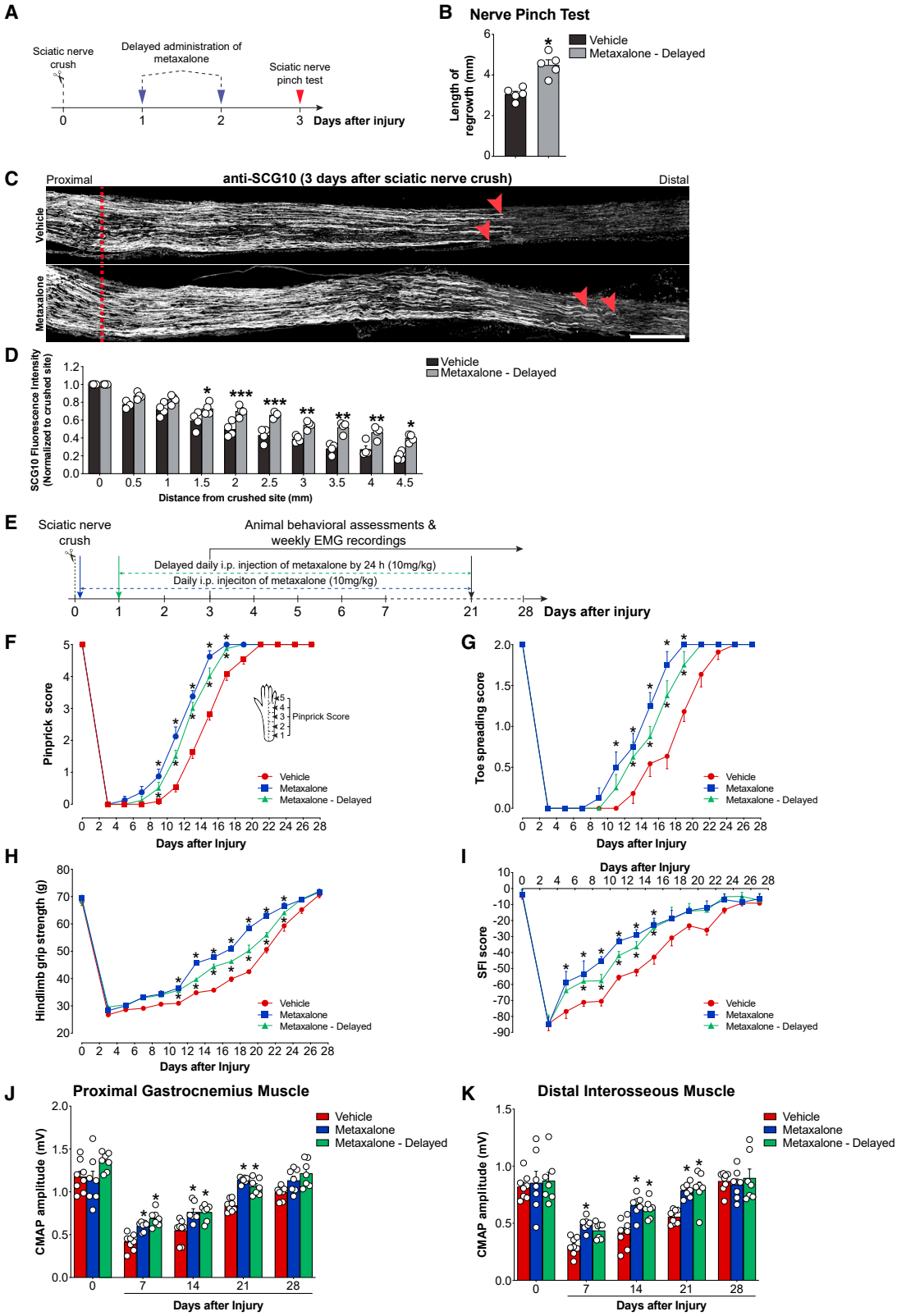

(legend on next page)

to pinprick stimuli (reaching score 1) as soon as on day 9 and day 10 post-injury, respectively. Mice regained full sensory pinprick response 4 days (metaxalone-treated) and 2 days (delayed-metaxalone-treated) earlier than vehicle controls (Figure 7F). For motor function recovery, metaxalone-treated mice took 14 days to recover 50% of toe-spreading reflex (reaching score 1) and 19 days to fully regain toe-spreading reflex. Delayed-metaxalone-treated mice took 1 more day than metaxalone-treated mice to recover 50% of toe-spreading reflex as well as to fully regain toe-spreading reflex. The vehicle-treated mice were only able to recover 50% of toe-spreading reflex in 18 days and required 7 more days to fully recover (Figure 7G). Metaxalone-treated and delayed-metaxalone-treated mice exhibited significantly higher hindlimb grip strength recovery than controls from days 11 to 23 (Figure 7H). Metaxalone and delayed metaxalone treatment displayed the most rapid SFI improvement over the course of recovery after injury compared with vehicle alone. At 15 days post-injury (halfway through the recovery period), the average SFI was increased substantially in mice treated with metaxalone immediately (73.0%) and delayed metaxalone treatment by 24 h (71.4%), whereas the average SFI of vehicle-treated mice was increased by 49.3% when compared with the SFI values at day 3 post-injury (Figure 7I).

Consistent with the animal behavioral data, EMG recordings of metaxalone-treated and delayed-metaxalone-treated mice in the proximal gastrocnemius revealed significant improvement in muscle activities at weeks 1–3 post-injury, when compared with the vehicle controls. The increase in muscle activity of metaxalone-treated mice reached significance levels in the most distal interosseous muscles during the first 3 weeks post-injury, whereas a significant increase in muscle activity was detected in delayed-metaxalone-treated mice at weeks 2–3 post-injury compared with vehicle controls (Figures 7J and 7K). In conclusion, our bioinformatic analysis successfully identified an FDA-approved small-molecule metaxalone that not only recapitulated the growth-promoting effects of *Fmn2* ablation in peripheral nerve repair but was also able to delay intervention by such a large therapeutic time window, which is advantageous in the translation of findings into clinical application.

DISCUSSION

This work reveals that neuronal *Fmn2* deletion promotes axon regeneration and function recovery by increasing microtubule dynamics and post-translational modification such as tubulin deacetylation at the distal ends of growing axons. Fmn2 has been shown to bind and interact with microtubule and to induce α-tubulin acetylation.[73,75] Tubulin deacetylation, which is induced by HDAC, produces highly dynamic microtubules and plays a key role in axon regeneration.[23] However, little is known about the mechanisms underpinning Fmn2 function in peripheral nerve regeneration. In this study, we first examined the potential beneficial effects of LDIR on *in vitro* and *in vivo* axonal regrowth in axotomized DRG neurons. We hypothesize that the alternation in gene expression profiling following LDIR contributes to the beneficial adaptive responses after PNI. However, our RRBS and transcriptional analysis showed that LDIR did not affect the global DNA methylation and key RAG expression in axotomized DRG neurons. There is a lack of consistent correlation between the DNA methylation and RAG expression.[17–20] For instance, either pharmacological induction or suppression of global DNA methylation reduces neurite outgrowth in axotomized DRG neurons by suppressing gene expression of a number of key RAGs, including *Arg1*, *Sprr1a*, *Gadd45a*, and *Gap43*.[19] We, therefore, performed an in-depth bioinformatics analysis to reveal a previously unrecognized functional role of Fmn2, with over 96% of DNA hypermethylation occurring in its promoter region (downregulation of Fmn2 expression), in axon regeneration. Our RNA-seq analysis showed that ablation of *Fmn2* did not alter RAG expression in injured DRGs, but interestingly, *Fmn2* deletion induced activation of transcriptional networks regulating immune responses such as the Jak-Stat signaling pathway, and pathways involved in chemokine and cytokine production were uniquely enriched only in injured $Fmn2^{-/-}$ DRGs. It is well documented that STAT3, which acts as a transcription factor mediating virtually all cytokine-driven signaling, is a critical transforming factor of the neuronal pro-regenerative state.[82–84] Our GSEA suggests that *Fmn2* deletion might create a favorable anti-inflammatory microenvironment for peripheral nerve repair. We then confirmed that the injury-induced Fmn2 downregulation in DRGs at the early time points after injury whereas robust axon regeneration occurs.[1,3,4] Using a combination of approaches, we causally demonstrate the relationship between the *Fmn2* deletion and microtubule dynamics and the acceleration of axon regeneration and function recovery.

Microtubule plus-end polymerization is required for regenerating axons through cycles of polymerization and depolymerization (dynamic instability), which allows microtubules at the growing ends to probe the intracellular environment and to facilitate the projection of regenerating axons back to their original target areas (i.e., skin and muscle).[22] Microtubule dynamic instability is, therefore, critical for growth cone guidance, guiding the regenerating

Figure 7. Delay metaxalone treatment still promotes robust *in vivo* axon regeneration and function recovery after PNI

(A) Metaxalone (0.25 μg/μL) was administered to the site of injury 1 day after sciatic nerve crush for 2 consecutive days (twice per day with an 8-h time interval).

(B) Delayed metaxalone treatment by 24 h was as effective as regular metaxalone treatment in promoting *in vivo* axon regeneration (n = 5 per group). Each dot represents the length of axonal regrowth per mouse.

(C) Delayed metaxalone treatment regrew more and longer SCG10-positive regenerating axons than controls. Dotted line: site of injury. Arrowhead: distal regenerating axons. Scale bars, 500 μm.

(D) Regeneration index was measured (n = 4 per group). Each dot represents normalized SCG10 immunoreactivity per mouse.

(E) Experimental paradigm for delayed metaxalone treatment.

(F–I) Both metaxalone-treated and delayed-metaxalone-treated mice displayed acceleration of sensory (F) and motor (G–I) function recovery to similar extents (n = 8–11 per group).

(J and K) Significant increase in CMAP amplitudes in proximal (gastrocnemius; J) and distal plantar (interosseous; K) muscles were observed after injury. (n = 7–8 per group.) Each dot represents the average CMAP amplitude per mouse. Mean ± SEM. *p < 0.05, **p < 0.01, ***p < 0.001; Student's t test for (B), two-way ANOVA with post hoc Bonferroni test for (D), two-way ANOVA with repeated measures, followed by Bonferroni's post hoc test for (F)–(K).

axons along their correct path.[85,86] In this study, we show that *Fmn2* deletion prolongs the high microtubule dynamic phase at the microtubule plus ends of growing axons by increasing the speed of microtubule polymerization (growth velocity) and duration of microtubule polymerization (growth length). We also hypothesize that following microtubule polymerization, post-translational modifications would have a direct effect on microtubule dynamics via tubulin acetylation. Our data show that pHDAC5 was highly upregulated exclusively at the regenerating axons of AAV2/9-*Fmn2*-shRNA mice 3 days after sciatic nerve crush. Inhibition of HDAC5 activity through either LMK-235 or gene silencing of *Hdac5* using AAV2/9-*Hdac5*-shRNA, both treatments eliminated the axon growth-promoting effect of *Fmn2* deletion completely in AAV2/9-*Fmn2*-shRNA mice (Figures 4B and 4C). Our results agree well with the observation that peripheral axonal injury induced nuclear export of HDAC5 from the nucleus to the cytoplasm and subsequent HDAC5 anterograde transport into the axons.[76] Additionally, HDAC5, but not HDAC1-4 and 6, is identified as a novel injury-dependent tubulin deacetylase catalyzing the deacetylation of α-tubulin in axons.[23] By inhibiting the expression of HDAC6 and pharmacologically blocking HDAC6 activity, neurite outgrowth in cortical neurons is improved on inhibitory substrates of myelin, such as myelin-associated glycoprotein and chondroitin sulfate proteoglycan.[87] However, the promoting effect of HDAC6 in permissive PNS microenvironment is negligible, and HDAC6 knockdown has no significant effect on axon regeneration.[23] Unlike HDAC6, HDAC5 knockdown in DRG neurons does not affect the basal level of acetylated tubulin, indicating that HDAC5 is not involved in regulating tubulin acetylation under basal conditions but only in response to injury. Whereas sciatic nerve injury induces phosphorylation (activation) of HDAC5 in injured axons *in vivo*, relatively low pHDAC5 expression was detected in the uninjured axons.[23] Recent reports also highlight the fact that increased tubulin polymerization and microtubule dynamics show promising results for axon regeneration and function recovery after injury.[88] For instance, genetic ablation of βIII-tubulin (TUBB3) markedly elevated the level of acetylated tubulin (stable form) and impaired microtubule polymerization at the growth cones of cultured DRG neurons. The reduced microtubule dynamics impaired neurite outgrowth of TUBB3-deficient neurons, resulting in delayed sensory function recovery after PNI.[22] Epothilone B induced rapid tubulin polymerization at the growing tips of cultured rat cortical neurons and promoted *in vivo* axon regeneration after spinal cord injury.[89] Similarly, paclitaxel-induced active tubulin polymerization at the growth cones[90] and facilitated *in vivo* axon regeneration and partial function recovery in rats with spinal cord injury.[91] Nevertheless, chronic exposure to epothilone B or paclitaxel is known to cause chemotherapy-induced peripheral neuropathy when used at high doses in animals.[92,93] It is also notable that formin protein has been known as an actin nucleator and plays a key role in formin-dependent actin nucleation, which is the first step in actin polymerization.[94] Understanding the changes in actin cytoskeleton in the growth cone of *Fmn2*-deficient neurons and the involvement of Fmn2 in actin-microtubule crosstalk would be an important area for further research on axon regeneration.[95–97]

In the final proof-of-concept experiment, we performed a small-molecule bioinformatics analysis using the gene expression profile signature of $Fmn2^{-/-}$ to query a public database, LINCS, which consists of 44,328 bioactive small molecules and 1,234 of them are FDA-approved small molecules.[98,99] We identified metaxalone, an FDA-approved drug, which has been used as a skeletal muscle relaxant to treat a broad range of skeletal muscle disorders associated with acute and painful musculoskeletal conditions (i.e., diabetic neuropathy) for over 2 decades.[100–102] Additionally, we demonstrated that metaxalone treatment delayed by 24 h post-injury can still accelerate substantial axon regeneration and function recovery to a level comparable to that of metaxalone treatment immediately after injury, which provides a highly relevant treatment strategy for clinical setting.

Taken together, this study provides novel insights into the development of an FDA-approved small-molecule-based therapy for treating PNIs. It usually takes over 15 years from the identification of bioactive compound to FDA approval for clinical application. Repurposing an existing FDA-approved drug such as metaxalone would be so time saving that normally phase I clinical trials can be skipped. This is an important proof-of-concept study to demonstrate that FDA-approved small molecules identified by bioinformatics analysis can be readily used as a potential therapy not only for PNIs, which can also be applied to transitional drug discovery across a range of different nervous system disorders.

STAR★METHODS

Detailed methods are provided in the online version of this paper and include the following:

- KEY RESOURCES TABLE
- RESOURCE AVAILABILITY
  - Lead contact
  - Materials availability
  - Data and code availability
- EXPERIMENTAL MODEL AND STUDY PARTICIPANT DETAILS
  - Animals
  - Method details Surgery
  - Whole-body X-ray irradiation
  - *Ex vivo* DRG explant culture
  - Primary dissociated DRG culture
  - Alpha-particle and X-ray irradiation on cultured DRG neurons
  - Neurite outgrowth and cell survival assays
  - Genomic DNA extraction and reduced representation bisulfite sequencing (RRBS)
  - Total RNA extraction and qPCR analysis
  - AAV2/9-mediated *in vivo* knockdown of *Fmn2* and *Hdac5* expression
  - Sciatic nerve pinch test
  - Quantification of *in vivo* axon regeneration
  - Sensory and motor function recovery tests
  - Electromyography (EMG) recording
  - Immunohistochemistry analysis of the neuron specific AAV serotype tropism in DRGs, sciatic nerves, and lumbar ventral horn motor neurons
  - Fluorescence activated cell sorting (FACS)
  - Western blot analysis

- Live-cell imaging and analysis of microtubule dynamics at the growth cone of DRG neurons
- HDAC5 inhibitor LMK-235 treatment
- RNA-seq whole transcriptome analysis
- Functional enrichment analysis
- *In silico* small molecule screening
- Assessment of small molecules for *in vivo* axon regeneration and function recovery after PNI
- Statistical analysis

SUPPLEMENTAL INFORMATION

Supplemental information can be found online at https://doi.org/10.1016/j.neuron.2023.11.011.

ACKNOWLEDGMENTS

This work was supported in part by the Research Grant Council of the Hong Kong Special Administrative Region (HKSAR) Government (CityU 11100417 and CityU 11100519) and the Health Bureau, HKSAR Government (07181356), awarded to C.H.E.M., and by the Shenzhen Science, Technology, and Innovation Commission (project no. 基2020N368) and the Research Grants Council (11103619, C4024-22GF) of the HKSAR Government, awarded to X.W.

AUTHOR CONTRIBUTIONS

N.P.B.A. performed DRG cultures, AAV injections, qPCR, western blot analysis, sciatic nerve pinch tests, histology, animal behavior assessment, and electrophysiology experiments. X.C. performed animal behavior assessments on metaxalone-treated mice. Y.T.Y.L. performed animal behavior assessment on AAV2/9-*Fmn2*-shRNA mice. W.Y.T. performed RRBS on cultured DRG neurons after α-particle and X-ray irradiation. W.Y.T. and F.G. performed bioinformatic analysis on RNA-seq and RRBS. X.W., D.H.G., and G.C. provided expertise in bioinformatic analysis. C.H.E.M. conceived the project. C.H.E.M. and N.P.B.A. wrote the manuscript.

DECLARATION OF INTERESTS

C.H.E.M. and N.P.B.A. filed a patent on the use of Fmn2-shRNA and small molecules for the treatment of PNI (U.S. patent application 63/590,594).

Received: October 26, 2022
Revised: September 2, 2023
Accepted: November 10, 2023
Published: December 11, 2023

REFERENCES

1. Ma, C.H., Brenner, G.J., Omura, T., Samad, O.A., Costigan, M., Inquimbert, P., Niederkofler, V., Salie, R., Sun, C.C., Lin, H.Y., et al. (2011). The BMP coreceptor RGMb promotes while the endogenous BMP antagonist noggin reduces neurite outgrowth and peripheral nerve regeneration by modulating BMP signaling. J. Neurosci. *31*, 18391–18400.
2. Korngut, L., Ma, C.H., Martinez, J.A., Toth, C.C., Guo, G.F., Singh, V., Woolf, C.J., and Zochodne, D.W. (2012). Overexpression of human HSP27 protects sensory neurons from diabetes. Neurobiol. Dis. *47*, 436–443.
3. Ma, C.H., Omura, T., Cobos, E.J., Latrémolière, A., Ghasemlou, N., Brenner, G.J., van Veen, E., Barrett, L., Sawada, T., Gao, F., et al. (2011). Accelerating axonal growth promotes motor recovery after peripheral nerve injury in mice. J. Clin. Invest. *121*, 4332–4347.
4. Asthana, P., Zhang, G., Sheikh, K.A., and Him Eddie Ma, C. (2021). Heat shock protein is a key therapeutic target for nerve repair in autoimmune peripheral neuropathy and severe peripheral nerve injury. Brain Behav. Immun. *91*, 48–64.
5. Asthana, P., Kumar, G., Milanowski, L.M., Au, N.P.B., Chan, S.C., Huang, J., Feng, H., Kwan, K.M., He, J., Chan, K.W.Y., et al. (2022). Cerebellar glutamatergic system impacts spontaneous motor recovery by regulating Gria1 expression. NPJ Regen. Med. *7*, 45.
6. Lang, B.T., Wang, J., Filous, A.R., Au, N.P., Ma, C.H., and Shen, Y. (2014). Pleiotropic molecules in axon regeneration and neuroinflammation. Exp. Neurol. *258*, 17–23.
7. Cobos, E.J., Nickerson, C.A., Gao, F., Chandran, V., Bravo-Caparrós, I., González-Cano, R., Riva, P., Andrews, N.A., Latremoliere, A., Seehus, C.R., et al. (2018). Mechanistic differences in neuropathic pain modalities revealed by correlating behavior with global expression profiling. Cell Rep. *22*, 1301–1312.
8. Au, N.P.B., Kumar, G., Asthana, P., Gao, F., Kawaguchi, R., Chang, R.C.C., So, K.F., Hu, Y., Geschwind, D.H., Coppola, G., and Ma, C.H.E. (2022). Clinically relevant small-molecule promotes nerve repair and visual function recovery. NPJ Regen. Med. *7*, 50.
9. Au, N.P., Kumar, G., Asthana, P., Tin, C., Mak, Y.L., Chan, L.L., Lam, P.K., and Ma, C.H. (2016). Ciguatoxin reduces regenerative capacity of axotomized peripheral neurons and delays functional recovery in pre-exposed mice after peripheral nerve injury. Sci. Rep. *6*, 26809.
10. Kumar, G., Au, N.P., Lei, E.N., Mak, Y.L., Chan, L.L., Lam, M.H., Lam, P.K., and Ma, C.H. (2016). Acute exposure to pacific ciguatoxin reduces electroencephalogram activity and disrupts neurotransmitter metabolic pathways in motor cortex. Mol. Neurobiol. *54*, 5590–5603.
11. Hwang, J.Y., Aromolaran, K.A., and Zukin, R.S. (2017). The emerging field of epigenetics in neurodegeneration and neuroprotection. Nat. Rev. Neurosci. *18*, 347–361.
12. Lardenoije, R., Iatrou, A., Kenis, G., Kompotis, K., Steinbusch, H.W., Mastroeni, D., Coleman, P., Lemere, C.A., Hof, P.R., van den Hove, D.L., and Rutten, B.P. (2015). The epigenetics of aging and neurodegeneration. Prog. Neurobiol. *131*, 21–64.
13. Rizk, E., Madrid, A., Koueik, J., Sun, D., Stewart, K., Chen, D., Luo, S., Hong, F., Papale, L.A., Hariharan, N., et al. (2023). Purified regenerating retinal neurons reveal regulatory role of DNA methylation-mediated Na+/K+-ATPase in murine axon regeneration. Commun. Biol. *6*, 120.
14. Reverdatto, S., Prasad, A., Belrose, J.L., Zhang, X., Sammons, M.A., Gibbs, K.M., and Szaro, B.G. (2022). Developmental and Injury-induced Changes in DNA Methylation in Regenerative versus Non-regenerative Regions of the Vertebrate Central Nervous System. BMC Genomics *23*, 2.
15. Oh, Y.M., Mahar, M., Ewan, E.E., Leahy, K.M., Zhao, G., and Cavalli, V. (2018). Epigenetic regulator UHRF1 inactivates REST and growth suppressor gene expression via DNA methylation to promote axon regeneration. Proc. Natl. Acad. Sci. USA *115*, E12417–E12426.
16. Weng, Y.L., An, R., Cassin, J., Joseph, J., Mi, R., Wang, C., Zhong, C., Jin, S.G., Pfeifer, G.P., Bellacosa, A., et al. (2017). An intrinsic epigenetic barrier for functional axon regeneration. Neuron *94*, 337–346.e6.
17. Puttagunta, R., Tedeschi, A., Sória, M.G., Hervera, A., Lindner, R., Rathore, K.I., Gaub, P., Joshi, Y., Nguyen, T., Schmandke, A., et al. (2014). PCAF-dependent epigenetic changes promote axonal regeneration in the central nervous system. Nat. Commun. *5*, 3527.
18. Loh, Y.E., Koemeter-Cox, A., Finelli, M.J., Shen, L., Friedel, R.H., and Zou, H. (2017). Comprehensive mapping of 5-hydroxymethylcytosine epigenetic dynamics in axon regeneration. Epigenetics *12*, 77–92.
19. Shin, H.Y., Kim, K., Kwon, M.J., Oh, Y.J., Kim, E.H., Kim, H.S., Hong, C.P., Lee, J.H., Lee, K., and Kim, B.G. (2020). Alteration in global DNA methylation status following preconditioning injury influences axon growth competence of the sensory neurons. Exp. Neurol. *326*, 113177.
20. Shin, J.E., and Cho, Y. (2017). Epigenetic regulation of axon regeneration after neural injury. Mol. Cells *40*, 10–16.

21. Iskandar, B.J., Rizk, E., Meier, B., Hariharan, N., Bottiglieri, T., Finnell, R.H., Jarrard, D.F., Banerjee, R.V., Skene, J.H., Nelson, A., et al. (2010). Folate regulation of axonal regeneration in the rodent central nervous system through DNA methylation. J. Clin. Invest. *120*, 1603–1616.

22. Latremoliere, A., Cheng, L., DeLisle, M., Wu, C., Chew, S., Hutchinson, E.B., Sheridan, A., Alexandre, C., Latremoliere, F., Sheu, S.H., et al. (2018). Neuronal-specific TUBB3 is not required for normal neuronal function but is essential for timely axon regeneration. Cell Rep. *24*, 1865–1879.e9.

23. Cho, Y., and Cavalli, V. (2012). HDAC5 is a novel injury-regulated tubulin deacetylase controlling axon regeneration. EMBO J. *31*, 3063–3078.

24. Cambray-Deakin, M.A., and Burgoyne, R.D. (1987). Posttranslational modifications of alpha-tubulin: acetylated and detyrosinated forms in axons of rat cerebellum. J. Cell Biol. *104*, 1569–1574.

25. Cho, Y., and Cavalli, V. (2014). HDAC signaling in neuronal development and axon regeneration. Curr. Opin. Neurobiol. *27*, 118–126.

26. Eira, J., Magalhães, J., Macedo, N., Pero, M.E., Misgeld, T., Sousa, M.M., Bartolini, F., and Liz, M.A. (2021). Transthyretin promotes axon growth via regulation of microtubule dynamics and tubulin acetylation. Front. Cell Dev. Biol. *9*, 747699.

27. Lin, S., Sterling, N.A., Junker, I.P., Helm, C.T., and Smith, G.M. (2017). Effects of alphaTAT1 and HDAC5 on axonal regeneration in adult neurons. PLoS One *12*, e0177496.

28. Song, Y., and Brady, S.T. (2015). Post-translational modifications of tubulin: pathways to functional diversity of microtubules. Trends Cell Biol. *25*, 125–136.

29. Tanaka, E., Ho, T., and Kirschner, M.W. (1995). The role of microtubule dynamics in growth cone motility and axonal growth. J. Cell Biol. *128*, 139–155.

30. Conde, C., and Cáceres, A. (2009). Microtubule assembly, organization and dynamics in axons and dendrites. Nat. Rev. Neurosci. *10*, 319–332.

31. Janke, C., and Kneussel, M. (2010). Tubulin post-translational modifications: encoding functions on the neuronal microtubule cytoskeleton. Trends Neurosci. *33*, 362–372.

32. Ertürk, A., Hellal, F., Enes, J., and Bradke, F. (2007). Disorganized microtubules underlie the formation of retraction bulbs and the failure of axonal regeneration. J. Neurosci. *27*, 9169–9180.

33. Luckey, T.D. (1982). Physiological benefits from low levels of ionizing radiation. Health Phys. *43*, 771–789.

34. Jiang, H., Li, W., Li, X., Cai, L., and Wang, G. (2008). Low-dose radiation induces adaptive response in normal cells, but not in tumor cells: in vitro and in vivo studies. J. Radiat. Res. *49*, 219–230.

35. Calabrese, E.J., and Baldwin, L.A. (2003). Toxicology rethinks its central belief. Nature *421*, 691–692.

36. Calabrese, E.J., Iavicoli, I., and Calabrese, V. (2013). Hormesis: its impact on medicine and health. Hum. Exp. Toxicol. *32*, 120–152.

37. Kaiser, J. (2003). Hormesis. Sipping from a poisoned chalice. Science *302*, 376–379.

38. Maisin, J.R., Gerber, G.B., Vankerkom, J., and Wambersie, A. (1996). Survival and diseases in C57BL mice exposed to X rays or 3.1 MeV neutrons at an age of 7 or 21 days. Radiat. Res. *146*, 453–460.

39. Ina, Y., and Sakai, K. (2004). Prolongation of life span associated with immunological modification by chronic low-dose-rate irradiation in MRL-lpr/lpr mice. Radiat. Res. *161*, 168–173.

40. Le Bourg, E. (2009). Hormesis, aging and longevity. Biochim. Biophys. Acta *1790*, 1030–1039.

41. Ott, O.J., Niewald, M., Weitmann, H.D., Jacob, I., Adamietz, I.A., Schaefer, U., Keilholz, L., Heyd, R., and Muecke, R.; German Cooperative Group on Radiotherapy for Benign Diseases (GCG-BD) (2015). DEGRO guidelines for the radiotherapy of non-malignant disorders. Part II: Painful degenerative skeletal disorders. Strahlenther. Onkol. *191*, 1–6.

42. Jacobs, P., and King, H.S. (1987). A randomized prospective comparison of chemotherapy to total body irradiation as initial treatment for the indolent lymphoproliferative diseases. Blood *69*, 1642–1646.

43. Kim, S., Nam, Y., Kim, C., Lee, H., Hong, S., Kim, H.S., Shin, S.J., Park, Y.H., Mai, H.N., Oh, S.M., et al. (2020). Neuroprotective and anti-inflammatory effects of low-moderate dose ionizing radiation in models of Alzheimer's disease. Int. J. Mol. Sci. *21*, 3678.

44. Cuttler, J.M., Moore, E.R., Hosfeld, V.D., and Nadolski, D.L. (2016). Treatment of Alzheimer disease with CT scans: A case report. Dose. Response *14*, 1559325816640073.

45. Jiang, B., Zhang, Y., Zhao, J., She, C., Zhou, X., Dong, Q., and Wang, P. (2017). Effects of localized X-ray irradiation on peripheral nerve regeneration in transected sciatic nerve in rats. Radiat. Res. *188*, 455–462.

46. Pogribny, I., Raiche, J., Slovack, M., and Kovalchuk, O. (2004). Dose-dependence, sex- and tissue-specificity, and persistence of radiation-induced genomic DNA methylation changes. Biochem. Biophys. Res. Commun. *320*, 1253–1261.

47. Kovalchuk, O., Burke, P., Besplug, J., Slovack, M., Filkowski, J., and Pogribny, I. (2004). Methylation changes in muscle and liver tissues of male and female mice exposed to acute and chronic low-dose X-ray-irradiation. Mutat. Res. *548*, 75–84.

48. Koturbash, I., Miousse, I.R., Sridharan, V., Nzabarushimana, E., Skinner, C.M., Melnyk, S.B., Pavliv, O., Hauer-Jensen, M., Nelson, G.A., and Boerma, M. (2016). Radiation-induced changes in DNA methylation of repetitive elements in the mouse heart. Mutat. Res. *787*, 43–53.

49. Newman, M.R., Sykes, P.J., Blyth, B.J., Bezak, E., Lawrence, M.D., Morel, K.L., and Ormsby, R.J. (2014). The methylation of DNA repeat elements is sex-dependent and temporally different in response to X radiation in radiosensitive and radioresistant mouse strains. Radiat. Res. *181*, 65–75.

50. Wang, J., Zhang, Y., Xu, K., Mao, X., Xue, L., Liu, X., Yu, H., Chen, L., and Chu, X. (2014). Genome-wide screen of DNA methylation changes induced by low dose X-ray radiation in mice. PLoS One *9*, e90804.

51. De Virgiliis, F., Hutson, T.H., Palmisano, I., Amachree, S., Miao, J., Zhou, L., Todorova, R., Thompson, R., Danzi, M.C., Lemmon, V.P., et al. (2020). Enriched conditioning expands the regenerative ability of sensory neurons after spinal cord injury via neuronal intrinsic redox signaling. Nat. Commun. *11*, 6425.

52. Kong, G., Zhou, L., Serger, E., Palmisano, I., De Virgiliis, F., Hutson, T.H., McLachlan, E., Freiwald, A., La Montanara, P., Shkura, K., et al. (2020). AMPK controls the axonal regenerative ability of dorsal root ganglia sensory neurons after spinal cord injury. Nat. Metab. *2*, 918–933.

53. Weng, Y.L., Wang, X., An, R., Cassin, J., Vissers, C., Liu, Y., Liu, Y., Xu, T., Wang, X., Wong, S.Z.H., et al. (2018). Epitranscriptomic m(6)A regulation of axon regeneration in the adult mammalian nervous system. Neuron *97*, 313–325.e6.

54. Howell, G.R., Soto, I., Zhu, X., Ryan, M., Macalinao, D.G., Sousa, G.L., Caddle, L.B., MacNicoll, K.H., Barbay, J.M., Porciatti, V., et al. (2012). Radiation treatment inhibits monocyte entry into the optic nerve head and prevents neuronal damage in a mouse model of glaucoma. J. Clin. Invest. *122*, 1246–1261.

55. Au, N.P.B., Chand, R., Kumar, G., Asthana, P., Tam, W.Y., Tang, K.M., Ko, C.C., and Ma, C.H.E. (2022). A small molecule M1 promotes optic nerve regeneration to restore target-specific neural activity and visual function. Proc. Natl. Acad. Sci. USA *119*, e2121273119.

56. Chine, V.B., Au, N.P.B., and Ma, C.H.E. (2019). Therapeutic benefits of maintaining mitochondrial integrity and calcium homeostasis by forced expression of Hsp27 in chemotherapy-induced peripheral neuropathy. Neurobiol. Dis. *130*, 104492.

57. Asthana, P., Zhang, N., Kumar, G., Chine, V.B., Singh, K.K., Mak, Y.L., Chan, L.L., Lam, P.K.S., and Ma, C.H.E. (2018). Pacific ciguatoxin induces excitotoxicity and neurodegeneration in the motor cortex via

caspase 3 activation: implication for irreversible motor deficit. Mol. Neurobiol. *55*, 6769–6787.

58. Arthur-Farraj, P.J., Morgan, C.C., Adamowicz, M., Gomez-Sanchez, J.A., Fazal, S.V., Beucher, A., Razzaghi, B., Mirsky, R., Jessen, K.R., and Aitman, T.J. (2017). Changes in the coding and non-coding transcriptome and DNA methylome that define the Schwann cell repair phenotype after nerve injury. Cell Rep. *20*, 2719–2734.
59. Wan, J., Oliver, V.F., Wang, G., Zhu, H., Zack, D.J., Merbs, S.L., and Qian, J. (2015). Characterization of tissue-specific differential DNA methylation suggests distinct modes of positive and negative gene expression regulation. BMC Genomics *16*, 49.
60. Chandran, V., Coppola, G., Nawabi, H., Omura, T., Versano, R., Huebner, E.A., Zhang, A., Costigan, M., Yekkirala, A., Barrett, L., et al. (2016). A systems-level analysis of the peripheral nerve intrinsic axonal growth program. Neuron *89*, 956–970.
61. Dumont, J., Million, K., Sunderland, K., Rassinier, P., Lim, H., Leader, B., and Verlhac, M.H. (2007). Formin-2 is required for spindle migration and for the late steps of cytokinesis in mouse oocytes. Dev. Biol. *301*, 254–265.
62. Kwon, S., Shin, H., and Lim, H.J. (2011). Dynamic interaction of formin proteins and cytoskeleton in mouse oocytes during meiotic maturation. Mol. Hum. Reprod. *17*, 317–327.
63. Leader, B., and Leder, P. (2000). Formin-2, a novel formin homology protein of the cappuccino subfamily, is highly expressed in the developing and adult central nervous system. Mech. Dev. *93*, 221–231.
64. Leader, B., Lim, H., Carabatsos, M.J., Harrington, A., Ecsedy, J., Pellman, D., Maas, R., and Leder, P. (2002). Formin-2, polyploidy, hypofertility and positioning of the meiotic spindle in mouse oocytes. Nat. Cell Biol. *4*, 921–928.
65. Pfender, S., Kuznetsov, V., Pleiser, S., Kerkhoff, E., and Schuh, M. (2011). Spire-type actin nucleators cooperate with Formin-2 to drive asymmetric oocyte division. Curr. Biol. *21*, 955–960.
66. Chang, L.L., Wang, H.C., Tseng, K.Y., Su, M.P., Wang, J.Y., Chuang, Y.T., Wang, Y.H., and Cheng, K.I. (2020). Upregulation of miR-133a-3p in the sciatic nerve contributes to neuropathic pain development. Mol. Neurobiol. *57*, 3931–3942.
67. Kudo, M., Wupuer, S., Fujiwara, M., Saito, Y., Kubota, S., Inoue, K.I., Takada, M., and Seki, K. (2021). Specific gene expression in unmyelinated dorsal root ganglion neurons in nonhuman primates by intra-nerve injection of AAV 6 vector. Mol. Ther. Methods Clin. Dev. *23*, 11–22.
68. Bradke, F., Fawcett, J.W., and Spira, M.E. (2012). Assembly of a new growth cone after axotomy: the precursor to axon regeneration. Nat. Rev. Neurosci. *13*, 183–193.
69. Stout, A., D'Amico, S., Enzenbacher, T., Ebbert, P., and Lowery, L.A. (2014). Using plusTipTracker software to measure microtubule dynamics in Xenopus laevis growth cones. J. Vis. Exp. *91*, e52138.
70. Applegate, K.T., Besson, S., Matov, A., Bagonis, M.H., Jaqaman, K., and Danuser, G. (2011). plusTipTracker: Quantitative image analysis software for the measurement of microtubule dynamics. J. Struct. Biol. *176*, 168–184.
71. Kundu, T., Dutta, P., Nagar, D., Maiti, S., and Ghose, A. (2021). Coupling of dynamic microtubules to F-actin by Fmn2 regulates chemotaxis of neuronal growth cones. J. Cell Sci. *134*, jcs252916.
72. Chesarone, M.A., DuPage, A.G., and Goode, B.L. (2010). Unleashing formins to remodel the actin and microtubule cytoskeletons. Nat. Rev. Mol. Cell Biol. *11*, 62–74.
73. Quinlan, M.E., Hilgert, S., Bedrossian, A., Mullins, R.D., and Kerkhoff, E. (2007). Regulatory interactions between two actin nucleators, Spire and Cappuccino. J. Cell Biol. *179*, 117–128.
74. Rosales-Nieves, A.E., Johndrow, J.E., Keller, L.C., Magie, C.R., Pinto-Santini, D.M., and Parkhurst, S.M. (2006). Coordination of microtubule and microfilament dynamics by Drosophila Rho1, Spire and Cappuccino. Nat. Cell Biol. *8*, 367–376.
75. Thurston, S.F., Kulacz, W.A., Shaikh, S., Lee, J.M., and Copeland, J.W. (2012). The ability to induce microtubule acetylation is a general feature of formin proteins. PLoS One *7*, e48041.
76. Cho, Y., Sloutsky, R., Naegle, K.M., and Cavalli, V. (2013). Injury-induced HDAC5 nuclear export is essential for axon regeneration. Cell *155*, 894–908.
77. Marek, L., Hamacher, A., Hansen, F.K., Kuna, K., Gohlke, H., Kassack, M.U., and Kurz, T. (2013). Histone deacetylase (HDAC) inhibitors with a novel connecting unit linker region reveal a selectivity profile for HDAC4 and HDAC5 with improved activity against chemoresistant cancer cells. J. Med. Chem. *56*, 427–436.
78. Higuchi, F., Uchida, S., Yamagata, H., Abe-Higuchi, N., Hobara, T., Hara, K., Kobayashi, A., Shintaku, T., Itoh, Y., and Suzuki, T. (2016). Hippocampal microRNA-124 enhances chronic stress resilience in mice. J. Neurosci. *36*, 7253–7267.
79. Zhou, W., Yang, J., Saren, G., Zhao, H., Cao, K., Fu, S., Pan, X., Zhang, H., Wang, A., and Chen, X. (2020). HDAC6-specific inhibitor suppresses Th17 cell function via the HIF-1alpha pathway in acute lung allograft rejection in mice. Theranostics *10*, 6790–6805.
80. Omura, T., Omura, K., Tedeschi, A., Riva, P., Painter, M.W., Rojas, L., Martin, J., Lisi, V., Huebner, E.A., Latremoliere, A., et al. (2015). Robust axonal regeneration occurs in the injured CAST/Ei Mouse CNS. Neuron *86*, 1215–1227.
81. Kandasamy, K., Gowdra, V., Nammalvar, H., and Govindarajan, A. (2012). Bioanalytical method development, validation and quantification of metaxalone in rat plasma by liquid chromatography tandem mass spectrometry. J. Bioanal. Biomed. *S6*, 2.
82. Smith, R.P., Lerch-Haner, J.K., Pardinas, J.R., Buchser, W.J., Bixby, J.L., and Lemmon, V.P. (2011). Transcriptional profiling of intrinsic PNS factors in the postnatal mouse. Mol. Cell. Neurosci. *46*, 32–44.
83. Zigmond, R.E. (2011). gp130 cytokines are positive signals triggering changes in gene expression and axon outgrowth in peripheral neurons following injury. Front. Mol. Neurosci. *4*, 62.
84. Bareyre, F.M., Garzorz, N., Lang, C., Misgeld, T., Büning, H., and Kerschensteiner, M. (2011). In vivo imaging reveals a phase-specific role of STAT3 during central and peripheral nervous system axon regeneration. Proc. Natl. Acad. Sci. USA *108*, 6282–6287.
85. Dent, E.W., and Gertler, F.B. (2003). Cytoskeletal dynamics and transport in growth cone motility and axon guidance. Neuron *40*, 209–227.
86. Rolls, M.M., Thyagarajan, P., and Feng, C. (2021). Microtubule dynamics in healthy and injured neurons. Dev. Neurobiol. *81*, 321–332.
87. Rivieccio, M.A., Brochier, C., Willis, D.E., Walker, B.A., D'Annibale, M.A., McLaughlin, K., Siddiq, A., Kozikowski, A.P., Jaffrey, S.R., Twiss, J.L., et al. (2009). HDAC6 is a target for protection and regeneration following injury in the nervous system. Proc. Natl. Acad. Sci. USA *106*, 19599–19604.
88. Blanquie, O., and Bradke, F. (2018). Cytoskeleton dynamics in axon regeneration. Curr. Opin. Neurobiol. *51*, 60–69.
89. Ruschel, J., Hellal, F., Flynn, K.C., Dupraz, S., Elliott, D.A., Tedeschi, A., Bates, M., Sliwinski, C., Brook, G., Dobrindt, K., et al. (2015). Axonal regeneration. Systemic administration of epothilone B promotes axon regeneration after spinal cord injury. Science *348*, 347–352.
90. Witte, H., Neukirchen, D., and Bradke, F. (2008). Microtubule stabilization specifies initial neuronal polarization. J. Cell Biol. *180*, 619–632.
91. Hellal, F., Hurtado, A., Ruschel, J., Flynn, K.C., Laskowski, C.J., Umlauf, M., Kapitein, L.C., Strikis, D., Lemmon, V., Bixby, J., et al. (2011). Microtubule stabilization reduces scarring and causes axon regeneration after spinal cord injury. Science *331*, 928–931.
92. Tamburin, S., Park, S.B., Alberti, P., Demichelis, C., Schenone, A., and Argyriou, A.A. (2019). Taxane and epothilone-induced peripheral neurotoxicity: from pathogenesis to treatment. J. Peripher. Nerv. Syst. *24*, S40–S51.

93. Chine, V.B., Au, N.P.B., Kumar, G., and Ma, C.H.E. (2019). Targeting axon integrity to prevent chemotherapy-induced peripheral neuropathy. Mol. Neurobiol. *56*, 3244–3259.

94. Pruyne, D., Evangelista, M., Yang, C., Bi, E., Zigmond, S., Bretscher, A., and Boone, C. (2002). Role of formins in actin assembly: nucleation and barbed-end association. Science *297*, 612–615.

95. Stern, S., Hilton, B.J., Burnside, E.R., Dupraz, S., Handley, E.E., Gonyer, J.M., Brakebusch, C., and Bradke, F. (2021). RhoA drives actin compaction to restrict axon regeneration and astrocyte reactivity after CNS injury. Neuron *109*, 3436–3455.e9.

96. Tedeschi, A., Dupraz, S., Curcio, M., Laskowski, C.J., Schaffran, B., Flynn, K.C., Santos, T.E., Stern, S., Hilton, B.J., Larson, M.J.E., et al. (2019). ADF/cofilin-mediated actin turnover promotes axon regeneration in the adult CNS. Neuron *103*, 1073–1085.e6.

97. Henty-Ridilla, J.L., Rankova, A., Eskin, J.A., Kenny, K., and Goode, B.L. (2016). Accelerated actin filament polymerization from microtubule plus ends. Science *352*, 1004–1009.

98. Stathias, V., Jermakowicz, A.M., Maloof, M.E., Forlin, M., Walters, W., Suter, R.K., Durante, M.A., Williams, S.L., Harbour, J.W., Volmar, C.H., et al. (2018). Drug and disease signature integration identifies synergistic combinations in glioblastoma. Nat. Commun. *9*, 5315.

99. Wang, Z., Lachmann, A., Keenan, A.B., and Ma'ayan, A. (2018). L1000FWD: fireworks visualization of drug-induced transcriptomic signatures. Bioinformatics *34*, 2150–2152.

100. Dent, R.W., Jr., and Ervin, D.K. (1975). A study of metaxalone (Skelaxin) vs. placebo in acute musculoskeletal disorders: a cooperative study. Curr. Ther. Res. Clin. Exp. *18*, 433–440.

101. Fathie, K. (1964). A second look at a skeletal muscle relaxant: A double-blind study of metaxalone. Curr. Ther. Res. Clin. Exp. *6*, 677–683.

102. Pfeifer, M.A., Ross, D.R., Schrage, J.P., Gelber, D.A., Schumer, M.P., Crain, G.M., Markwell, S.J., and Jung, S. (1993). A highly successful and novel model for treatment of chronic painful diabetic peripheral neuropathy. Diabetes Care *16*, 1103–1115.

103. Krueger, F., and Andrews, S.R. (2011). Bismark: a flexible aligner and methylation caller for bisulfite-seq applications. Bioinformatics *27*, 1571–1572.

104. Langmead, B., and Salzberg, S.L. (2012). Fast gapped-read alignment with Bowtie 2. Nat. Methods *9*, 357–359.

105. Akalin, A., Kormaksson, M., Li, S., Garrett-Bakelman, F.E., Figueroa, M.E., Melnick, A., and Mason, C.E. (2012). methylKit: a comprehensive R package for the analysis of genome-wide DNA methylation profiles. Genome Biol. *13*, R87.

106. Kandimalla, R., Ozawa, T., Gao, F., Wang, X., and Goel, A.; T1 Colorectal Cancer Study Group (2019). Gene expression signature in surgical tissues and endoscopic biopsies identifies high-risk T1 colorectal cancers. Gastroenterology *156*, 2338–2341.e3.

107. Kong, E.Y., Cheng, S.H., and Yu, K.N. (2016). Biphasic and triphasic dose responses in zebrafish embryos to low-dose 150 kV X-rays with different levels of hardness. J. Radiat. Res. *57*, 363–369.

108. Kong, E.Y., Yeung, W.K., Chan, T.K., Cheng, S.H., and Yu, K.N. (2016). Exogenous nitric oxide suppresses in vivo X-ray-induced targeted and non-targeted effects in zebrafish embryos. Int. J. Mol. Sci. *17*, 1321.

109. Au, N.P., Fang, Y., Xi, N., Lai, K.W., and Ma, C.H. (2014). Probing for chemotherapy-induced peripheral neuropathy in live dorsal root ganglion neurons with atomic force microscopy. Nanomedicine *10*, 1323–1333.

110. Yum, E.H., Li, V.W., Choi, V.W., Cheng, S.H., and Yu, K.N. (2010). Effects of alpha particles on zebrafish embryos. Appl. Radiat. Isot. *68*, 714–717.

111. Huang, H., Hu, J., Maryam, A., Huang, Q., Zhang, Y., Ramakrishnan, S., Li, J., Ma, H., Ma, V.W.S., Cheuk, W., et al. (2021). Defining super-enhancer landscape in triple-negative breast cancer by multiomic profiling. Nat. Commun. *12*, 2242.

112. Recalde, M., Gárate-Rascón, M., Herranz, J.M., Elizalde, M., Azkona, M., Unfried, J.P., Boix, L., Reig, M., Sangro, B., Fernández-Barrena, M.G., et al. (2022). DNA methylation regulates a set of long non-coding RNAs compromising hepatic identity during hepatocarcinogenesis. Cancers (Basel) *14*, 2048.

113. Skjærven, K.H., Jakt, L.M., Fernandes, J.M.O., Dahl, J.A., Adam, A.C., Klughammer, J., Bock, C., and Espe, M. (2018). Parental micronutrient deficiency distorts liver DNA methylation and expression of lipid genes associated with a fatty-liver-like phenotype in offspring. Sci. Rep. *8*, 3055.

114. Cheng, D., Deng, J., Zhang, B., He, X., Meng, Z., Li, G., Ye, H., Zheng, S., Wei, L., Deng, X., et al. (2018). LncRNA HOTAIR epigenetically suppresses miR-122 expression in hepatocellular carcinoma via DNA methylation. EBiomedicine *36*, 159–170.

115. Lindner, R., Puttagunta, R., Nguyen, T., and Di Giovanni, S. (2014). DNA methylation temporal profiling following peripheral versus central nervous system axotomy. Sci. Data *1*, 140038.

116. Tam, W.Y., Au, N.P., and Ma, C.H. (2016). The association between laminin and microglial morphology in vitro. Sci. Rep. *6*, 28580.

117. Tam, W.Y., and Ma, C.H. (2014). Bipolar/rod-shaped microglia are proliferating microglia with distinct M1/M2 phenotypes. Sci. Rep. *4*, 7279.

118. Shin, J.E., Geisler, S., and DiAntonio, A. (2014). Dynamic regulation of SCG10 in regenerating axons after injury. Exp. Neurol. *252*, 1–11.

119. Sun, F., Park, K.K., Belin, S., Wang, D., Lu, T., Chen, G., Zhang, K., Yeung, C., Feng, G., Yankner, B.A., and He, Z. (2011). Sustained axon regeneration induced by co-deletion of PTEN and SOCS3. Nature *480*, 372–375.

120. Kalinski, A.L., Yoon, C., Huffman, L.D., Duncker, P.C., Kohen, R., Passino, R., Hafner, H., Johnson, C., Kawaguchi, R., Carbajal, K.S., et al. (2020). Analysis of the immune response to sciatic nerve injury identifies efferocytosis as a key mechanism of nerve debridement. eLife *9*, e60223.

121. Ashburner, M., Ball, C.A., Blake, J.A., Botstein, D., Butler, H., Cherry, J.M., Davis, A.P., Dolinski, K., Dwight, S.S., Eppig, J.T., et al. (2000). Gene ontology: tool for the unification of biology. The Gene Ontology Consortium. Nat. Genet. *25*, 25–29.

122. Kanehisa, M., and Goto, S. (2000). KEGG: kyoto encyclopedia of genes and genomes. Nucleic Acids Res. *28*, 27–30.

123. Wang, X., Terfve, C., Rose, J.C., and Markowetz, F. (2011). HTSanalyzeR: an R/Bioconductor package for integrated network analysis of high-throughput screens. Bioinformatics *27*, 879–880.

124. Kucera, M., Isserlin, R., Arkhangorodsky, A., and Bader, G.D. (2016). AutoAnnotate: A Cytoscape app for summarizing networks with semantic annotations. F1000Res *5*, 1717.

STAR★METHODS

KEY RESOURCES TABLE

REAGENT or RESOURCE	SOURCE	IDENTIFIER
Antibodies		
Mouse anti-βIII-tubulin	Sigma Aldrich	Cat# T8660; RRID: AB_477590
Mouse anti-GAPDH	ProteinTech	Cat# 60004-1-Ig; RRID: AB_2107436
Mouse anti-acetylated Tubulin	Sigma Aldrich	Cat# T7451; RRID: AB_609894
Mouse anti-α-tubulin	Sigma Aldrich	Cat# T8203; RRID: AB_1841230
Mouse anti-NeuN	Millipore	Cat# MAB377; RRID: AB_2298772
Mouse anti-GFP	Cell Signaling Technology	Cat# 2956; RRID: AB_1196615
Rabbit anti-FMN2	ProteinTech	Cat# 11259-1-AP; RRID: AB_2105250
Rabbit anti-SCG10	Novus Biologicals	Cat# NBP1-49461; RRID: AB_10011569
Rabbit phospho-HDAC5 (Ser498)	Thermo Fisher Scientific	Cat# PA5-37779; RRID: AB_2554387
Rabbit anti-HDAC5	Novus Biologicals	Cat# NBP2-22152
Rabbit anti-SOX10	Abcam	Cat# ab180862; RRID: AB_2721184
Rabbit anti-CD68	Abcam	Cat# ab213363; RRID: AB_2801637
Rabbit anti-IBA-1	FUJIFILM Wako Shibayagi	Cat# 019-19741; RRID: AB_839504
Goat anti-Choline Acetyltransferase (ChAT)	Millipore	Cat# AB144P; RRID: AB_2079751
Goat anti-Mouse IgG (H+L) Cross-Adsorbed Secondary Antibody, Alexa Fluor™ 488	Thermo Fisher Scientific	Cat# A-11001; RRID: AB_2534069
Goat anti-Mouse IgG (H+L) Cross-Adsorbed Secondary Antibody, Alexa Fluor™ 555	Thermo Fisher Scientific	Cat# A-21422; RRID: AB_2535844
Goat anti-Mouse IgG (H+L) Cross-Adsorbed Secondary Antibody, Alexa Fluor™ 647	Thermo Fisher Scientific	Cat# A-21235; RRID: AB_2535804
Goat anti-Rabbit IgG (H+L) Cross-Adsorbed Secondary Antibody, Alexa Fluor™ 488	Thermo Fisher Scientific	Cat# A-11008; RRID: AB_143165
Goat anti-Rabbit IgG (H+L) Cross-Adsorbed Secondary Antibody, Alexa Fluor™ 555	Thermo Fisher Scientific	Cat# A-21428; RRID: AB_2535849
Goat anti-Rabbit IgG (H+L) Cross-Adsorbed Secondary Antibody, Alexa Fluor™ 647	Thermo Fisher Scientific	Cat# A-21244; RRID: AB_2535812
Donkey anti-Goat IgG (H+L) Cross-Adsorbed Secondary Antibody, Alexa Fluor™ 555	Thermo Fisher Scientific	Cat# A-21432; RRID: AB_2535853
Goat anti-Mouse IgG (H+L) Secondary Antibody, HRP	Thermo Fisher Scientific	Cat# 31430; RRID: AB_228307
Goat anti-Rabbit IgG (H+L) Secondary Antibody, HRP	Thermo Fisher Scientific	Cat# 32460, RRID: AB_1185567
Bacterial and virus strains		
pAAV-U6-shRNA1(Fmn2)-U6-shRNA2(Fmn2)-U6-shRNA3(Fmn2)-CMV-EGFP-WPRE	This paper	N/A
pAAV-U6-shRNA1(Hdac5)-U6-shRNA2(Hdac5)-U6-shRNA3(Hdac5)-CMV-EGFP-WPRE	This paper	N/A
pAAV-U6-shRNA(scr)-CMV-EGFP-WPRE	Au et al.[55]	N/A
pAAV-CAG-EB3-mCherry-WPRE-SV40pA	This paper	N/A
Chemicals, peptides, and recombinant proteins		
Cytosine β-D-arabinofuranoside hydrochloride (Ara-C)	Sigma Aldrich	Cat# C6645-25MG
B27	Gibco	Cat# 10889-038
Collagenase A	Roche	Cat# 10103578001
Dispase II	Roche	Cat# 04942078001
GDNF	Sigma Aldrich	Cat# G1401-10UG

(*Continued on next page*)

Continued

REAGENT or RESOURCE	SOURCE	IDENTIFIER
Heat-inactivated FBS	Gibco	Cat# 10082-147
Laminin	Sigma Aldrich	Cat# L2020-1MG
NGF 2.5S	Gibco	Cat# 13257-019
Penicillin-Streptomycin (10,000 U/mL)	Gibco	Cat# 15140-122
Poly-D-lysine	Sigma Aldrich	Cat# P6407-5MG
L-Glutamine	Gibco	Cat# 25030-149
Matrigel	BD Biosciences	Cat# 356234
Trypsin	Gibco	Cat# 15050-065
Bovine Serum Albumin	Sigma Aldrich	Cat# A9418-10G
Neurobasal Medium	Gibco	Cat# 21103-049
DMEM Medium	Gibco	Cat# 11995-065
Paraformaldehyde	Sigma Aldrich	Cat# 158127-500G
Triton X-100	Sigma Aldrich	Cat# T8787
Optimal Cutting Temperature compound	SAKURA	Cat# 4583
DAPI	Thermo Fisher Scientific	Cat# D1306
Trizma® base	Sigma Aldrich	Cat# T6066-500G
Sodium chloride	Sigma Aldrich	Cat# S3014-1KG
0.5M EDTA	Thermo Fisher Scientific	Cat# 15575-020
SDS	Bio-Rad	Cat# 161-0301
DTT	Sigma Aldrich	Cat# 43816-10ML
PMSF	Sigma Aldrich	Cat# P7626-250MG
cOmplete™, Mini, EDTA-free Protease Inhibitor Cocktail	Roche	Cat# 11836170001
Phosphatase Inhibitor Cocktail 2	Sigma Aldrich	Cat# P5726-1ML
Phosphatase Inhibitor Cocktail 3	Sigma Aldrich	Cat# P0044-1ML
Tris-Glycine SDS Sample Buffer	Thermo Fisher Scientific	Cat# LC2676
Tris-Glycine SDS Running Buffer	Thermo Fisher Scientific	Cat# LC2675
Tris Buffered Saline (TBS)	Bio-Rad	Cat# 1706435
Tween 20	Bio-Rad	Cat# 1706531
SuperSignal™ West Femto Maximum Sensitivity Substrate	Thermo Fisher Scientific	Cat# 34095
RNAiso Plus	Takara	Cat# 9108
LMK-235	Selleck Chemicals	Cat# S7569-10mg
Alverine	Sigma Aldrich	Cat# A0424
Cilnidipine	Sigma Aldrich	Cat# C1493
Metaxalone	Sigma Aldrich	Cat# SML0199
Acamprosate	Sigma Aldrich	Cat# A6981
Critical commercial assays		
WST-1 cell proliferation assay kit	ClonTech	Cat# 630118
Superscript III First-Strand Synthesis SuperMix	Invitrogen	Cat# 18080-400
KAPA SYBR Fast qPCR Kit	KAPA	Cat# KK4602
PureLink Genomic DNA Mini Kit	Invitrogen	Cat# K182001
Deposited data		
Raw and analyzed data	This paper	GEO: GSE243896
Experimental models: Organisms/strains		
Mouse: C57BL/6J	The Jackson Laboratory	N/A
Mouse: 129S6-*Fmn2*^{tm1Led}/RwwJ	Leader et al.[64]	Strain #:016264; RRID: IMSR_JAX:016264Info

(*Continued on next page*)

Continued		
REAGENT or RESOURCE	SOURCE	IDENTIFIER
Oligonucleotides		
qPCR primer sequence: see Table S4	This paper	N/A
shRNA sequence: see Table S5	This paper	N/A
Software and algorithms		
Prism 9	GraphPad	https://www.graphpad.com/features
ImageJ	NIH	RRID: SCR_002285
MATLAB	Mathworks	https://www.mathworks.com/products/matlab.html
RStudio	R Foundation	N/A
WIS-NeuroMath	Ma et al.[3]	N/A
Image Lab	Bio-rad	https://www.bio-rad.com/en-uk/product/image-lab-software?ID=KRE6P5E8Z
Spike2	Cambridge Electronic Design	https://ced.co.uk/products/spkovin
NIS-Elements	Nikon Instruments	https://www.microscope.healthcare.nikon.com/products/software/nis-elements
plusTipTracker	Applegate et al.[70]	https://cloud.biohpc.swmed.edu/index.php/s/NghaDz2GQY90BSs/download
Bismark	Krueger and Andrews[103]	https://github.com/FelixKrueger/Bismark
bowtie2	Langmead and Salzberg[104]	https://github.com/BenLangmead/bowtie2
methylKit	Akalin et al.[105]	https://github.com/al2na/methylKit
DEseq2	Kandimalla et al.[106]	https://bioconductor.org/packages/release/bioc/html/DESeq2.html
Library of Integrated Network-Based Cellular Signatures (LINCS)	Wang et al.[99]	N/A

RESOURCE AVAILABILITY

Lead contact

Further information and requests for resources and reagents should be directed to and will be fulfilled by the lead contact, Prof. Chi Him Eddie Ma (eddiema@cityu.edu.hk).

Materials availability

All unique/stable reagents generated in this study are available from the lead contact with a completed Materials Transfer Agreement.

Data and code availability

All data reported in this paper will be shared by the lead contact upon request. Sequencing data are deposited in Gene Expression Omnibus (GEO) under the accession number GSE243896 and publicly available as of the date of publication. The accession number is also listed in the key resources table. This paper does not report the original code. Any additional information required to reanalyze the data reported in this paper is available from the lead contact upon reasonable request.

EXPERIMENTAL MODEL AND STUDY PARTICIPANT DETAILS

Animals

Animal experiments were performed in accordance with the experimental procedures approved by the Animal Research Ethics Sub-Committee at the City University of Hong Kong. In compliance with the American Veterinary Medical Association (AVMA) Guidelines on euthanasia, carbon dioxide asphyxiation was performed for animal euthanasia. Adult male C57BL/6 or *Fmn2* knockout (Fmn2$^{-/-}$) mice (8-12 weeks old) were used in both *in vitro* and *in vivo* experiments. The mice were provided with food and water *ad libitum*, with a 12:12 h light-dark cycle.

Fmn2$^{-/-}$ mice with 129S6/SvEvTac background were obtained from Jackson laboratory. To delete *Fmn2*, a 1,300-base pair (bp) sequence for the proline-rich FH1 domain of *Fmn2* gene was replaced by a 1,257-bp neomycin-resistance gene followed by a stop codon to terminate transcription of *Fmn2*. Fmn2$^{-/-}$ mice were viable, and no morphological and functional deficits were observed in the nervous system. Male Fmn2$^{-/-}$ mice were fertile and decreased fertility was found in female Fmn2$^{-/-}$ mice.[64] Therefore, only male Fmn2$^{-/-}$ mice were used in current study. PCR genotyping was performed with genomic DNA isolated from the tail. Forward

5'-CTAATTGTGGCTGCCCTTGT-3' and reverse 5'-AGGTGGCAATGTCAGGATTC-3' primers were used for PCR amplification of wild-type *Fmn2* with product size of 318 bp. Forward 5'-CTTGGGTGGAGAGGCTATTC-3' and reverse 5'-AGGTGAGATGACAGGA GATC-3' primers were used for PCR amplification of mutant *Fmn2* with product size of 280 bp.

Method details

Surgery

Sciatic nerve crush or transection injury was performed in anesthetized adult male C57BL/6 or Fmn2$^{-/-}$ mice (8-12 weeks old) as previously described.[1,3–5,9,56,57] Briefly, the left sciatic nerve was exposed at mid-thigh level. For crush injury, the exposed nerve was crushed with smooth forceps (Dumont #5/45 Forceps, Fine Science Tools) at the sciatic notch for 15 s. For sciatic nerve transection, an epineural suture was first made at the level of external rotator muscle, just distal to the sciatic notch. The exposed nerve was then transected using a pair of ophthalmic microscissors just distal to the suture. After injury, the overlying muscle and skin were sutured using a 5-0 suture (Ethilon), and the mice were allowed to recover on a heated pad, and returned to their home cages after recovery. The surgeon was blinded to the genotypes and treatments.

Whole-body X-ray irradiation

Adult male C57BL/6 mice (8-12 weeks old) were irradiated by a cabinet irradiator X-Rad 320 (Precision X-Ray) at 200kV and 10mA equipped with a beam conditioning filter (1.5 mm Aluminum, 0.25 mm Copper and 0.75 mm Tin) at a focus-to-surface distance of 70 cm. To ensure that each mouse inside the pie cage received the same amount of radiation, dosimetry inside the pie cage was measured by a dosimeter before experiment.[107,108] During irradiation, pie cage was placed on a slowly rotating turntable to allow uniform distribution of X-ray irradiation. Mice received a single exposure to X-ray irradiation at different doses (1-5 Gy). Sham irradiated control mice were placed inside the irradiator without switching on the X-ray. *Ex vivo* DRG explant cultures were performed 5 days after the whole-body X-ray irradiation (see Figure S1F for detailed experimental paradigm). For sciatic nerve pinch test and function recovery assessment after PNI, whole-body X-ray irradiation was performed on the injured mice immediately after sciatic nerve crush injury (see Figures 1A and 1D for detailed experimental paradigm).

Ex vivo DRG explant culture

Ex vivo DRG explant cultures were prepared from adult (8-12 weeks old) male C57BL/6, Fmn2$^{-/-}$ mice and their age-matched WT littermates as described.[1,109] Briefly, DRGs were dissected out, cleaned of spinal and peripheral roots and plate onto 8-well chambers (Millipore) coated with poly-D-lysine (100 μg/ml) (Sigma-Aldrich) and a thin layer of Matrigel (BD Biosciences). The DRG explants were then incubated in full Neurobasal (NB) medium supplemented with B27, 200 mM L-glutamine, penicillin/streptomycin, 50 ng/ml NGF (Gibco), 2 ng/ml GDNF and 10 μM Ara-C (Sigma-Aldrich). After 48 h, DRG explant cultures were fixed with 4% paraformaldehyde (PFA), and immunostained with anti-βIII-tubulin antibody for neurite outgrowth assay.

Primary dissociated DRG culture

Primary cultures of dissociated DRG neurons were prepared from adult male C57BL/6 or Fmn2$^{-/-}$ mice (8-12 weeks old) and their age-matched WT littermates as described.[3,9,56,109] Briefly, DRGs were dissected out from the mice and mildly digested in collagenase/dispase II (Roche Diagnostics) solution, trypsinized and mechanically dissociated using flame polished Pasteur pipettes with three different diameters. DRG neurons were incubated in full NB medium.

For extraction of genomic DNA or total RNA from cultured DRG neurons, DRG neurons were plated on a thin layer of Mylar film (for alpha particle irradiation) or glass bottom dishes (for X-ray irradiation) pre-coated with poly-D-lysine (100 μg/ml) and laminin (10 μg/ml) (Sigma-Aldrich), at a fixed cell density of 3,000 cells/cm^2. The DRG neurons were cultured in Neurobasal (NB) medium supplemented with B27, 200 mM L-glutamine, penicillin/streptomycin, 50 ng/ml NGF (Gibco), 2 ng/ml GDNF and 10 μM Ara-C (Sigma-Aldrich) for 17 h.

Alpha-particle and X-ray irradiation on cultured DRG neurons

For α-particle irradiation, a planar ^{241}Am with α-particle energy of 5.49MeV under vacuum and activity of 4.26kBq was placed under a 9 mm-hole covered by Mylar film. DRG neurons were exposed to α-particle irradiation for 1 min, which corresponded to the absorbed dose of 20 mGy.[110] Sham irradiation was performed by exposing the neurons to a non-radioactive source (i.e. plastic film) for 1 min.

For X-ray irradiation, the glass bottom dish containing the DRG neurons were placed at the center of the X-ray irradiator and exposed to a single dose of 150 mGy, using a cabinet irradiator X-Rad 320 (Precision X-Ray) equipped with a beam conditioning filter (1.5 mm Aluminum, 0.25 mm Copper and 0.75 mm Tin) at a focus-to-surface distance (FSD) of 70 cm. Sham irradiation was performed by placing the cultured neurons at the center of the X-ray irradiator for 2.5 min (i.e. the duration of X-ray irradiation at 150 mGy) without switching on the machine. Alpha-particle and X-ray irradiation were performed 1 h after cell plating.

Neurite outgrowth and cell survival assays

For *ex vivo* DRG explant culture, non-overlapping quadrant images were taken from each DRG explant, and total neurite length was measured using automated WIS-NeuroMath software (Weizmann Institute of Science).[1,109] Data were obtained from at least 3 separate experiments with n = 8 explants per dose. For dissociated DRG cultures, DRG cultures were fixed with 4% paraformaldehyde

(PFA) after 17 h of incubation, blocked with 0.5% bovine serum albumin/0.1% Triton X-100 (Sigma-Aldrich), incubated with anti-βIII-tubulin (1:800; Sigma-Aldrich) and then incubated with corresponding secondary antibodies conjugated with Alexa Fluor 488 (1:300; Molecular Probes). Neurite outgrowth assay was performed as described.[3,9,56,93,109] Briefly, 30 non-overlapping images were taken at 10× magnifications using an epifluorescence microscope (Nikon Eclipse Ni-E) equipped with a motorized stage. Total neurite length and average longest neurite length were quantified using automated WIS-NeuroMath software (Weizmann Institute of Science). Data was obtained from 3 independent experiments repeated in duplicates. βIII-tubulin-positive DRG neurons with intact neurites adjacent to the neuronal cell bodies were counted as healthy neurons for neurite outgrowth assay.

Cell survival assay was performed using WST-1 reagents according to the manufacturer's instructions (ClonTech). Briefly, DRG neurons were plated onto a poly-D-lysine (100 μg/ml) and laminin (10 μg/ml) (Sigma-Aldrich)-coated 96-well plates at a cell density of 500 cells per well, and incubated in full NB medium. After LDIR treatments, 10 μl of WST-1 reagent was added into each well and incubated for another 3.5 h. The absorbance at 460 nm was determined using a microplate reader (BioTek Powerwave XS MQX200R). Data were obtained from three independent experiments repeated in triplicate.

Genomic DNA extraction and reduced representation bisulfite sequencing (RRBS)

After 17 h of incubation, α-particle-treated or X-ray-treated DRG neurons were trypsinzed and resuspended with the cell lysis buffer. Genomic DNA was isolated using PureLink Genomic DNA Mini Kit (Invitrogen). Genomic DNA was digested with MspI, and preceded to library preparation. After bisulfite conversion which converted the unmethylated cytosine nucleotides into uracil, while methylated cytosine nucleotides remained unmodified, the bisulfite converted DNA was amplified using PCR, and the amplified PCR fragments was sequenced using Illumia HiSeq 1500.

Bioinformatics analysis on RRBS was performed as previously described.[111] Briefly, raw reads of RRBS were first aligned to the mouse reference genome (UCSC GRCm38/mm10) using Bismark (version 0.13)[103] and bowtie2 (version 2.3.5)[104] program with default parameters. The resultant BAM files were then imported to the R package methylKit (version 1.2.10)[105] to calculate DNA methylation levels of promoter regions (5,000 bp upstream of the transcription start site) for each gene. Several studies suggested that differential methylation is strongly enriched at the promoter region (5,000 bp upstream of the transcription start site), and thus putative promoter sequence of the gene is likely to be found, and its expression is affected by DNA methylation at the promoter region.[112–115]

Total RNA extraction and qPCR analysis

After 17 h of incubation, total RNA was isolated from DRG cultures treated with 20 mGy of α-particle irradiation or with 150 mGy of X-ray irradiation, and their respective sham irradiated controls, using Trizol reagent (Invitrogen). Lumbar 4 and 5 (L4/5) DRG neurons directly supplying the sciatic nerve injury were harvested at various time points after sciatic nerve transection, and total RNA was extracted using Trizol reagent (Invitrogen). Reverse transcription was performed using Superscript III First-Strand Synthesis SuperMix (Invitrogen). Quantitative PCR (qPCR) were performed in triplicates using KAPA SYBR Fast qPCR Kit (KAPA) on QuantStudio 12K Flex Real-Time PCR System (Applied Biosystems). Gapdh was used as an endogenous control, and the relative fold change of each gene candidates was calculated using $2^{-\Delta\Delta ct}$ formula.[4,5,116,117] The qPCR primer sequences were listed in Table S4.

AAV2/9-mediated *in vivo* knockdown of *Fmn2* and *Hdac5* expression

For *in vivo* gene silencing of *Fmn2* and/or *Hdac5* in DRGs, AAV2/9-*Fmn2*-shRNA and AAV2/9-*Hdac5*-shRNA at a titer of 5×10^{12} vg/mL (OBiO Technology) were injected into the sciatic nerve directly through a glass micropipette using a microinjector (Harvard Apparatus) 2 weeks before sciatic nerve crush injury.[51,52,66,67] The mice were then subjected to sciatic nerve crush injury and sciatic nerve pinch test (Figure 4) and animal behavioral assessment (Figure S8). The expression of shRNAs was under the control of the U6 promoter, and the expression of the reporter gene eGFP was under the control of the CAG promoter. AAV2/9-scr-shRNA (Packgene) was used as a negative control (see Table S5 for the shRNA sequences). On a separate batch of animals, the knockdown efficiency in DRGs was assessed by western blot analysis in AAV2-*Fmn2*-shRNA and AAV2-*Hdac5*-shRNA mice 2 weeks after the AAV injection (Figures S8B and S9). To confirm the successful knockdown of Fmn2 in motor neurons, the lumbar ventral horns were harvested[3] from in AAV2-*Fmn2*-shRNA mice for western blot analysis (Figure S7D) and immunohistochemistry study (Figure S7E) 2 weeks after the AAV injection.

Sciatic nerve pinch test

Sciatic nerve pinch test was performed in the ipsilateral side 3 days after sciatic nerve crush injury. Mice were anesthetized under 2.5% isoflurane, and left sciatic nerve was exposed at the mid-thigh level. Mice were then slowly recovered under light anesthesia (1% isoflurane). A series of pinches were applied from the most distal part of the sciatic nerve near to the trifurcation, moving proximally to the crushed site, using smooth forceps (Dumont #5/45 Forceps, Fine Science Tools). The distance (in mm) representing the length of axonal regrowth was recorded from the crushed site to the most distal point of sciatic nerve whereas initial withdrawal reflex was observed after pinching.[1,3] The observers were blinded to the treatment and genotype.

Quantification of *in vivo* axon regeneration

Mice were perfused transcardially with 4% PFA, and L4/5 DRGs and sciatic nerves were harvested, post-fixed, cryoprotected and frozen in OCT compound (Tissue-Tek). For regenerating axon quantification, 12-μm thick longitudinal serial sections of sciatic nerve were blocked with 0.5% BSA/0.1% Triton X-100 (Sigma-Aldrich), and incubated with anti-SCG10 (a marker for regenerating sensory axons; 1:5,000; Novus Biologicals) primary antibodies. The sections were then incubated with secondary antibody conjugated with Alexa Fluor 555 (1:300; Molecular Probes). A series of z-stack images were taken at 20× magnifications using Nikon AXR confocal microscope equipped with a motorized stage and a resonant scanner, stitched, and maximally projected using NIS-Elements software.

To quantify regenerating axons, the SCG10 fluorescence intensity was measured at different distal distances away from the crush site using a line scan macro in ImageJ (NIH). A fluorescence intensity profile of SCG10 immunoreactivity was plotted by averaging the SCG10 intensity from 100 neighboring pixels and normalized to that measured in the crushed site with maximal SCG10 immunoreactivity.[16,53,55,118] For each mouse, at least 3 non-overlapping sections (at least 36 μm apart) were used and averaged from 12-15 sections per genotype or treatment group (n = 4-5 per genotype or treatment group).

Sensory and motor function recovery tests

Adult male *Fmn2*$^{-/-}$ mice (8–12 weeks old) and their age-matched WT littermates, or adult male C57BL/6 mice (for whole-body X-ray, AAV2/9-*Fmn2*-shRNA and metaxalone experiments) were trained and habituated one week before the sciatic nerve crush injury. After three independent training sessions (30 min per session with 2 days break), baseline values were taken, and sciatic nerve crush injury were performed one day after the baseline recordings. Function recovery was monitored for 30 days. On day 3 after the sciatic nerve crush, we first perform pinprick assay and followed by motor function assays every other day in a sequential manner (toe spreading, grip strength, and sciatic functional index) with 30 min apart from each test.[3–5,9,56,57] Animal behavioral tests were done blinded to the surgery and genotypes.

Pinprick assay

Mice were placed singly in small wire-mesh cages for 30-min habituation, an insect pin (Fine Science Tools) were applied to the lateral plantar surface of the ipsilateral hindlimb from toe to heel. The lateral planar surface was divided into 5 different areas, from the most distal toe (score = 5) to the heel (score = 1). The mouse was scored for that area if a brisk withdrawal response of hind paw was observed. The mouse was scored 0 if no withdrawal responses were observed after insect pin was applied to all 5 areas. Saphenous innervated area of the same hindlimb was tested as a positive control if there was no positive response from these five areas. Two rounds of pinprick assay were performed (with a 30-min time interval) in each mouse to confirm the score.[3–5,9,56]

Toe spreading reflex

To assess toe spreading reflex following PNI, mice were covered by a piece of cotton, lifted up by the tails, and uncovered their hindlimbs for assessment. Toe spreading reflex was scored as follow: 0 for no spreading, 1 for intermediate spreading with all toes separated for less than 2 s, and 2 for full spreading with all toes completely and widely spread, and sustained for at least 2 s. Mice were scored only when a full response was observed on the contralateral side (uninjured hindlimbs). Mice were assessed twice with 30-min time interval in between.[3–5,9,56]

Grip strength measurement

Muscle strength from hindlimbs were measured using a grip strength meter (BIO-GS3, Bioseb). To measure the grip strength of both hindlimbs, their hindlimbs were positioned to grip a metal T-bar connected to the grip strength meter, while their forelimbs were rested on a plastic bar. The mice were then gently pulled off from the T-bar. The values at which the mouse left the T-bar reflected the grip strength in grams. The average grip strength was taken from at least 5 consecutive grip strength measurements per animal.[4,5,9,56]

Sciatic functional index (SFI)

The walking track analysis was performed by training the mice to walk down a narrow corridor covered with white paper strip (10 x 60 cm) and the hindlimbs of the mice were pained with red water colour. SFI baseline values were taken after 3 independent training sessions spanning across the week before injury. The SFI values were calculated from footprints as follows:

-38.3 × (experimental print length - naive print length) / naive print length + 109.5 × (experimental toe spread - naive toe spread) / naive toe spread + 13.3 × (experimental intermediary toe spread - naive intermediary toe spread) / naive intermediary toe spread - 8.8. Print length was considered as the distance between the third toe to the heel. Toe spread was considered as the distance between the first and the fifth toe. Intermediary toe spread was considered as the distance between second and forth toe. Four clear and distinct footprints were taken from both the left injured ipsilateral experimental paw and the right uninjured contralateral naive paw for SFI calculation. Mice with SFI values close to 0 indicates normal gait movement, while the motor function is severely impaired if the SFI values close to -100.[4,5,9]

Electromyography (EMG) recording

Electromyography (EMG) recording was performed on anesthetized mice as described.[4,9,56,57] Briefly, mice were anesthetized with ketamine (100mg/kg)/xylazine (10mg/kg), and placed on a heat pad set to 37°C to avoid hypothermia during the course of EMG recordings. Baseline EMG were recorded before sciatic nerve crush injury using custom-made monopolar Teflon-coated electrodes. Following sciatic nerve crush injury, EMG were recorded on a weekly basis for one month (days 7, 14, 21 and 28). For EMG recordings of proximal gastrocnemius muscle, recording electrode was inserted into the gastrocnemius muscle, and Achilles tendon electrode

as a reference. For EMG recordings of distal interosseous muscle, recording electrode and reference electrode was inserted into first and fourth muscle of the same paw, respectively. Sciatic nerve was then stimulated proximally or distally, and both proximal and distal stimulations were used for CMAP of interosseous muscle. Only proximal stimulation was used for CMAP of the gastrocnemius muscle. The mean CMAP amplitude was recorded (Blackrock microsystem, USA) and calculated (Spike 2, UK).[3–5,9,56,57]

Immunohistochemistry analysis of the neuron specific AAV serotype tropism in DRGs, sciatic nerves, and lumbar ventral horn motor neurons

Two weeks after injection of AAV2/9-scr-shRNA (tagged with eGFP) into the sciatic nerves, mice were perfused transcardially with 4% PFA. Sciatic nerves, L4/5 DRGs, and lumbar ventral horn of spinal cords were harvested, post-fixed, cryoprotected, and frozen in OCT compound (Tissue-Tek). Five-micron-thick DRG cryosection, twelve-micron-thick longitudinal sciatic nerve cryosections, and thirty-micron-thick transverse spinal cord cryosections were blocked with 0.5% BSA/0.5% Triton X-100 (Sigma-Aldrich), and incubated with anti-βIII-tubulin (a neuronal marker; 1:800; Sigma-Aldrich), anti-ChAT (a motor neuron marker; 1:100; Millipore), anti-FMN2 (ProteinTech; 1:200), anti-SOX10 (a Schwann cell marker; 1:250; Abcam) or CD68 (a marker for macrophage; 1:250; Abcam) primary antibodies as indicated. The sections were then incubated with secondary antibodies conjugated with Alexa Fluor 555 (1:300; Molecular Probes) or Alexa Fluor 647 (1:300; Molecular Probes). For DRG and sciatic nerve cryosections, images were taken at 20× magnifications using Nikon Ni-E epifluorescence microscope equipped with a motorized stage (for DRG and sciatic nerve cryosections). For spinal cord cryosections, images were taken at 20× magnifications using Nikon AXR confocal microscope equipped with a motorized stage and resonant scanner.[1–3,9,56,57,93]

Fluorescence activated cell sorting (FACS)

Two weeks after injection of AAV2/9-scr-shRNA or AAV2/9-*Fmn2*-shRNA into the sciatic nerves, L4/5 DRGs were harvested, digested with collagenase/dispase, mechanically dissociated in dissociation buffer (1 × PBS with 10% FBS) using flame polished Pasteur pipettes with three different diameters, and then filtered through a 70-μm cell strainer (BD Falcon) to yield single cell suspension before FACS. All AAV2/9 used in the currently study were tagged with eGFP.

FACS was performed using SONY SH800Z Cell Sorter. To select DRG neurons, the dissociated cells were first separated based on the cell size (forward scatter) and cell surface characteristics (side scatter), and aggregated cells were eliminated based FSC-H:FSC-A ratio (Figure S7A). In each experiment, dissociated DRG neurons without AAV transduction were used as negative controls to set up the detection gate for eGFP-positive cells (Figure S7B).[119,120] The sorted eGFP-positive cells were immediately lysed and subjected to western blot analysis.

Western blot analysis

Ipsilateral L4/5 DRG neurons were harvested at various time points following sciatic nerve injury as indicated. Sciatic nerves were harvested 3 days after crush injury and segmented into 0–6 mm distal to the crush site.[23] Each protein sample was pooled from 3 mice. DRG neurons and segmented sciatic nerves were mechanically dissociated with protein lysis buffer, and subjected to measurement of protein concentration using protein BCA assay (Pierce). Protein lysate (30 μg) was separated on 4-12% NuPAGE Tris-Glycine precast gel (Invitrogen).[3,4,56,57,93] Protein was then transferred onto a PVDF membrane (Bio-Rad) and blocked with 5% non-fat milk (Bio-Rad) in TBS-T. The membrane was incubated with anti-FMN2 (1:500; ProteinTech), anti-phosphorylated HDAC5 (1:500, ThermoFisher), anti-HDAC5 (1:500, Novus Biologicals), anti-acetylated tubulin (1:10,000; Sigma-Aldrich), anti-NeuN (1:500; Millipore), anti-SOX10 (1:500; Abcam), anti-IBA-1 (1:1,000; Wako), anti-GFP (1:1,000; Cell Signaling), and anti-GAPDH antibodies (1:2,000; ProteinTech) as loading controls. The membrane was incubated with secondary antibody conjugated with horseradish peroxidase (1:2,000; Thermo-Fisher). Signals were detected using West Femto Maximum Sensitivity Substrate Kit (Thermo Scientific). The membrane was then stripped and re-blotted with anti-total tubulin antibodies (1:2,000; Sigma-Aldrich). Band intensities were measured using Image Lab software (Bio-Rad). FMN2 and pHDAC5 protein expression levels were normalized to GAPDH. Acetylated tubulin protein expression levels were first normalized to total tubulin levels, and then normalized to GAPDH.

Live-cell imaging and analysis of microtubule dynamics at the growth cone of DRG neurons

Two thousand DRG neurons were plated onto a poly-D-lysine and laminin-coated glass bottom dish,[3,55] and transduced with AAV2/9-EB3-mCherry (Packgene) 1 h after plating. On day 4 *in vitro*, EB3-mCherry tracking was performed and time-lapse images were taken at 100× magnifications using Nikon AXR confocal microscope equipped with a motorized stage and resonant scanner. Kymographs of EB3 comet motions at the growth cones were generated using NIS-Elements software.[55] For microtubule dynamics analysis, the EB3 comets at the growth cones were automatically traced and parameters of microtubule dynamics, including microtubule growth velocity, growth lifetime, growth length, and EB3 comet density, were determined using a MATLAB-based software plusTipTracker.[22,69,70] For each experimental group, at least 30 growth cones were analyzed from three independent experiments.

HDAC5 inhibitor LMK-235 treatment

To inhibit HDAC5-mediated tubulin deacetylation in mice, a selective inhibitor of HDAC4 and HDAC5, LMK-235 (20 mg/kg), was intraperitoneally injected into the adult male C57BL/6 mice (8-12 weeks old) pre-treated with AAV2/9-*Fmn2*-shRNA for 3 consecutive days.[23,77–79] The mice were then subjected to sciatic nerve pinch tests and immunohistochemistry analysis.

RNA-seq whole transcriptome analysis

Sciatic nerve transection was performed in adult male Fmn2$^{-/-}$ mice and WT littermates (8–12 weeks old), and L4/5 DRGs were harvested from both contralateral (uninjured) and ipsilateral (injured) sides 5 day after injury.[1,3] Total RNA was extracted using Trizol reagent, and 100 ng of total RNA from each sample (n = 3 per group) was used for library preparation after ribosomal RNA depletion. The library of each sample was then sequenced using Illumina Novaseq 6000 to a depth of 75 million reads per sample. After quality control using FastQC, sequencing data was mapped and annotated with the reference genome GRCm38, and quantified using DESeq. Genes with $\log_2$-fold > |1| and Benjamini-Hochberg adjusted $p < 0.05$ were considered as differentially expressed.[106] DESeq2 normalized counts with $\log_2$ transformation were used for principal component analysis and hierarchical clustering analysis.

Functional enrichment analysis

To examine the biological functions associated with differentially expressed genes in Fmn2$^{-/-}$ mice, GSEA and gene set overrepresentation analysis were performed on Gene Ontology (GO) gene sets (biological process, cellular component and molecular function categories)[121] and KEGG pathways[122] using 'HTSanalyzeR' R package.[123] Significantly enriched GO terms and pathways (Benjamini-Hochberg adjusted p value < 0.05) were clustered by AutoAnnotate (Version 1.3.2) with Markov Cluster method and visualized using Cytoscape (v.3.7.2).[124]

In silico small molecule screening

Library of Integrated Network-Based Cellular Signatures (LINCS) database was used for *in silico* small molecule screening. LINCS is a public web-based database which contains more than 1 million gene expression profiles derived from 50 human cell lines (including neuronal cell lines such as fibroblast-derived neuronal progenitor cells and terminally differentiated neurons) after treating with 44,328 bioactive small molecules (including 1,234 FDA-approved small molecules).[98,99] A total of 145 genes were uniquely differentially expressed only in injured Fmn2$^{-/-}$ DRG neurons and were used as query signature, compared with the gene expression profiles of neuronal cell lines in the public LINCS database. Based on a non-parametric, rank-based pattern-matching Kolmogorov-Smirnov statistics, each of the query signatures in the gene expression profile of injured Fmn2$^{-/-}$ DRG neurons was estimated with a metric, and the similarity of the query signature was evaluated with the gene expression profile derived from cell lines treated with small molecules (reference signatures).[60] This generated a connectivity score ranging from +100 (strong positive correlation) to -100 (strong negative correlation). The mean of the connectivity scores was used to rank the small molecules. Small molecules with connectivity score greater than +95 (strong overlapping between the query signatures and the reference signatures) were shortlisted for experimental validation (Table S2) using sciatic nerve pinch test in mice.[60]

Assessment of small molecules for *in vivo* axon regeneration and function recovery after PNI

To assess the promoting effects of top-ranked small molecules on *in vivo* axon regeneration, 40 μl of alverine (0.5 μg/μl), cilnidipine (0.5 μg/μl), metaxalone (0.25 μg/μl) or acamprosate (0.25 μg/μl) was administered directly to the site of injury of adult male C57BL/6 mice (8-12 weeks old) immediately after the sciatic nerve crush for 3 consecutive days (with both morning and evening dosing regimens over an 8-h time interval per day), given that the half-life of small molecules ranged from 5.7 to 33 h (i.e., metaxalone 9 h). The mice were then subjected to sciatic nerve pinch test and immunohistochemistry analysis.

To examine the therapeutic potential of metaxalone, adult mice received daily intraperitoneal injection of metaxalone at 10 mg/kg immediately after injury for 21 consecutive days (i.e., metaxalone treatment) or delaying daily intraperitoneal injection of metaxalone at 10 mg/kg to 24 h post-injury for 20 consecutive days (i.e., delayed metaxalone treatment), and all metaxalone treatments ended on day 21 post-injury. The mice were then subjected to sensory and motor function recovery tests and weekly EMG recordings for 28 days post-injury.

Statistical analysis

Data are presented as mean ± SEM. Student's t test (2 groups) or one-way ANOVA (more than 2 groups) followed by post hoc Bonferroni tests was used for data analysis where appropriate. Two-way ANOVA, followed by post hoc Bonferroni tests was used for the analysis of SCG10 immunoreactivity. Non-parametric Mann-Whitney U test (2 groups) or Kruskal-Wallis test followed by Dunn's post hoc tests (more than 2 groups) was used for the analysis of qPCR experiments. Two-way ANOVA with repeated measures, followed by post hoc Bonferroni tests was used for analysis of animal neurobehavioral and electrophysiological experiments. The microtubule growth velocity, microtubule growth length, microtubule growth lifetime, and the EB3 comet density were analyzed using Mann-Whitney U test. $p < 0.05$ was considered to be statistically significant. GraphPad Prism 9.0 was used for all the statistical analyses and graphing.